OXFORD

Cerebral Cortex, March 2021;31: 1444–1463

doi: 10.1093/cercor/bhaa282
Advance Access Publication Date: 29 October 2020
Feature Article

FEATURE ARTICLE

Structural and Functional Brain Parameters Related to Cognitive Performance Across Development: Replication and Extension of the Parieto-Frontal Integration Theory in a Single Sample

Ruben C. Gur[1,2,3], Ellyn R. Butler[1], Tyler M. Moore[1], Adon F.G. Rosen[1], Kosha Ruparel[1], Theodore D. Satterthwaite[1], David R. Roalf[1], Efstathios D. Gennatas[1], Warren B. Bilker[1,4], Russell T. Shinohara[4], Allison Port[1], Mark A. Elliott[1,2], Ragini Verma[2], Christos Davatzikos[2], Daniel H. Wolf[1], John A. Detre[3] and Raquel E. Gur[1,2,3]

[1]Brain Behavior Laboratory and the Neurodevelopment and Psychosis Section, Department of Psychiatry, University of Pennsylvania Perelman School of Medicine, Philadelphia, PA 19104, USA, [2]Department of Radiology, University of Pennsylvania Perelman School of Medicine, Philadelphia, PA 19104, USA, [3]Department of Neurology, University of Pennsylvania Perelman School of Medicine, Philadelphia, PA 19104, USA and [4]Department of Biostatistics, Epidemiology, and Informatics, University of Pennsylvania Perelman School of Medicine, Philadelphia, PA 19104, USA

Address correspondence to Ruben C. Gur, Brain Behavior Laboratory, University of Pennsylvania, 5th Floor Richards Building/Pod B, 3700 Hamilton Walk, Philadelphia, PA 19104, USA. Email: gur@upenn.edu.

Abstract

The parieto-frontal integration theory (PFIT) identified a fronto-parietal network of regions where individual differences in brain parameters most strongly relate to cognitive performance. PFIT was supported and extended in adult samples, but not in youths or within single-scanner well-powered multimodal studies. We performed multimodal neuroimaging in 1601 youths age 8–22 on the same 3-Tesla scanner with contemporaneous neurocognitive assessment, measuring volume, gray matter density (GMD), mean diffusivity (MD), cerebral blood flow (CBF), resting-state functional magnetic resonance imaging measures of the amplitude of low frequency fluctuations (ALFFs) and regional homogeneity (ReHo), and activation to a working memory and a social cognition task. Across age and sex groups, better performance was associated with higher volumes, greater GMD, lower MD, lower CBF, higher ALFF and ReHo, and greater activation for the working memory task in PFIT regions. However, additional cortical, striatal, limbic, and cerebellar regions showed comparable effects, hence PFIT needs expansion into an extended PFIT (ExtPFIT) network incorporating nodes that support motivation and affect. Associations of brain parameters became stronger with advancing age group from childhood to adolescence to young

adulthood, effects occurring earlier in females. This ExtPFIT network is developmentally fine-tuned, optimizing abundance and integrity of neural tissue while maintaining a low resting energy state.

Key words: multimodal neuroimaging, multimodal brain parameters, brain performance relation, neurodevelopment, neurocognition

Introduction

While multiple parameters of brain structure and function have been examined with structural and functional magnetic resonance imaging (MRI) studies, it is still unclear how these measures are related to arguably the main product of brain processes—cognitive performance. The relation between brain volume and cognitive performance has received the most extensive investigation since Frederick Tiedemann (1836) offered his conclusion that "There is undoubtedly a very close connexion between the absolute size of the brain and the intellectual powers and functions of the mind." (p. 502). However, the magnitude of this relation is still debated; estimates of the variance in cognitive measures explained by volume range from ~3% to > 30% (Witelson et al. 2006; Gignac and Bates 2017; Nave et al. 2019; Pietschnig et al. 2015). Advanced neuroimaging offers additional parameters of brain structure and function, and Jung and Haier (2007) performed a review of studies across modalities and proposed the parieto-frontal integration theory (PFIT), which stipulates a network of regions that are predominantly involved in complex reasoning and intelligence tasks. This network integrates dorsolateral prefrontal cortex, the inferior and superior parietal lobule (SPL), the anterior cingulate, and regions within the temporal (Tmp) and occipital (Occ) lobes (Basten et al. 2015; Estrada et al. 2019; Hilger et al. 2017). Within this network of regions, neuroanatomic parameters of higher volume, density and anisotropy and lower rates of cerebral blood flow (CBF) and metabolism have been associated with better cognitive performance.

The PFIT theory received some support in subsequent studies, although few have examined multiple brain parameters typically focusing only on volume. Ritchie et al. (2015) compared the relationship of volume to performance with other neuroanatomic parameters such as cortical thickness and found that volume accounted for the largest share of the variance (around 12%). Ryman et al. (2016) applied graph-theory analyses to volumetric data and reported that in males a latent factor of fronto-parietal gray matter (GM) related to general cognitive abilities, while in females the cognition-related factor involved white matter (WM) efficiency and total GM volume without regional specificity. Studies with relatively small samples have linked some diffusion tensor imaging (DTI) parameters to performance (e.g., Schmithorst et al. 2005; Qiu et al. 2008; Gençet al. 2018). A study on a larger sample ($N = 72$) applied graph theory to DTI data and reported sex differences, with females having greater local efficiency, but these effects were not linked to performance (Yan et al. 2011). Graph theory was also applied in the philadelphia neurodevelopmental cohort (PNC) sample by Ingalhalikar et al. (2014), and they reported greater within-hemispheric connectivity in males and between-hemispheric connectivity in females, as well as sex differences in modularity and participation coefficients.

Studies relating CBF to performance likewise supported the PFIT model, showing that age-related decline in CBF is related to performance decline (Hshieh et al. 2017; Rane et al. 2018). Resting-state functional MRI (rs_fMRI) was examined in relation to cognitive performance in a small sample (Pamplona et al. 2015), and in a larger sample ($N = 79$) by Vakhtin et al. (2014), who assessed both resting state and task-activated connectivity. They reported that regions involved in task-related networks included the bilateral medial frontal (Fro) and parietal (Par) cortex, right superior Fro lobule, and right cingulate gyrus. As part of multivariate measures in the Human Connectome Project (Smith et al. 2015), Finn et al. (2015) showed that functional connectivity profiles predicted "levels of fluid intelligence" and that "the same networks that were most discriminating of individuals were also most predictive of cognitive behavior." Furthermore, Yoo et al. (2018) reported, across several datasets, that models trained on task data outperformed those trained on resting-state data in predicting performance (cf. Fong et al. 2019; Jangraw et al. 2018) and Greene et al. (2018) demonstrated similar effects in two large datasets. Finally, Dubois et al. (2018) were able to predict up to 20% of the variance in general cognitive performance based on resting-state connectivity metrics in a large sample ($n = 884$) from the HCP. Each of these studies examined individual parameters of either structure or function. Therefore, there is a need for simultaneous examination of neuroanatomic and neurophysiologic parameters in relation to cognitive performance. Such simultaneous examination will allow gauging the relative contribution of the anatomic and physiologic parameters to cognitive performance, and their examination during development will offer insight on how brain parameters are fine-tuned for optimal adult levels. The PFIT has yet to be tested across both structural and functional brain parameters in a single, adequately powered multimodal study of youths.

We tested the PFIT with multimodal neuroimaging in a prospective sample of 1601 youths age 8–22, all studied on the same high-field (3 Tesla) scanner with contemporaneously obtained measures of cognitive performance, as part of the Philadelphia Neurodevelopmental Cohort (Gur et al. 2012; Calkins et al. 2015). The methods of sample ascertainment and the detailed neuroimaging protocols have been published (Satterthwaite et al. 2014a). Multimodal neuroimaging yielded regional measures of GM and WM volume and GM density (GMD) from T1-weighted scans, mean diffusivity (MD) from DTI (fractional anisotropy was also measured but since it is only valid in WM, this parameter was not included here), resting-state CBF from arterial spin-labeled (ASL) sequences, the amplitude of low frequency fluctuations (ALFFs) and regional homogeneity (ReHo) measures from rs_fMRI, and BOLD activation for a working-memory (NBack) and a social-cognition (emotion identification; IDEmo) task. The methods for image processing and for obtaining these brain parameters were detailed in previous publications (Gennatas et al. 2017; Ingalhalikar et al. 2014; Satterthwaite et al. 2014a,b; Vandekar et al. 2015) and are briefly summarized in the Methods section. The neurocognitive assessment provided measures of accuracy

Table 1 Intercorrelations among the global brain parameters for females (upper triangle) and males (lower triangle)

		Males								
		TBV	GMD	MD	CBF	ALFF	ReHo	NBack	IdEmo	N
Females	TBV		−0.018	−0.799***	0	0.086	0.079	0.072	0.118	603
	GMD	−0.001		0.192*	−0.322***	−0.087	−0.118	0.131	−0.122	603
	MD	−0.729***	0.3***		0.067	−0.027	−0.036	−0.045	−0.031	460
	CBF	−0.045	−0.175*	0.017		−0.019	0.004	−0.174	0.082	574
	ALFF	0.212***	−0.209***	−0.201**	0.075		0.767***	0.067	−0.007	405
	ReHo	0.103	−0.262***	−0.169*	0.068	0.715***		0.046	0.02	405
	NBack	0.145	0.05	−0.07	−0.026	0.032	−0.004		0.042	465
	IdEmo	0.154	−0.111	−0.077	0.029	0.026	0.084	0.165*		523
	N	677	677	560	649	500	500	550	611	

Note: *$P < 0.05$; **$P < 0.01$; ***$P < 0.001$. ALFF = Amplitude of low frequency fluctuations at resting-state; ReHo = Regional homogeneity at resting-state; Nback = Blood oxygenation-level dependent (BOLD) activation for the Nback task; IDEmo = BOLD activation for the emotion identification task.

and speed on multiple behavioral domains. Since available literature primarily examined general intellectual functioning, we selected as the primary cognitive measure the most comparable score from the battery, which is a factor score that summarizes accuracy on executive functioning and complex cognition (Moore et al. 2015; Swagerman et al. 2016).

Materials and Methods

Participants

Participants for the PNC were recruited from the Children's Hospital of Philadelphia pediatric network throughout the Delaware Valley as described in Calkins et al. (2015). A subsample of 1601 participants (out of the 9498 PNC sample) underwent multimodal neuroimaging, as described in Satterthwaite et al. (2014a). Of these, 340 were excluded for medical disorders that could affect brain function, as well as current use of psychoactive medications, prior inpatient psychiatric treatment, or an incidentally encountered structural brain abnormality. Sample size was further reduced for some modalities upon quality assurance procedures, most for excessive motion (see below, Table 1 and Supplementary Table S1). All participants underwent psychiatric assessment (Calkins et al. 2015) and neurocognitive testing (Gur et al. 2012, 2014).

Cognitive Measures

Cognitive performance was assessed with the Penn Computerized Neurocognitive Battery (CNB). The CNB consists of 14 tests adapted from tasks applied in functional neuroimaging to evaluate a range of cognitive domains (Gur et al. 2010, 2012, 2014; Moore et al. 2015; Roalf et al. 2014a). These domains include executive control (abstraction and mental flexibility, attention, working memory), episodic memory (verbal, facial, spatial), complex cognition (verbal reasoning, nonverbal reasoning, spatial processing), social cognition (emotion identification, emotion intensity differentiation, age differentiation) and sensorimotor and motor speed. Accuracy and speed for each test were z-transformed. Cognitive performance was summarized by a factor analysis of both speed and accuracy data (Moore et al. 2015), which delineated three accuracy factors corresponding to: 1) executive function and complex reasoning, 2) episodic memory, and 3) social cognition. The first factor was used as the measure of cognitive performance in all analyses, as it has the highest association with intelligence quotient (IQ) estimates (Moore et al. 2015; Swagerman et al. 2016).

Neuroimaging

All MRI scans were acquired on a single 3 T Siemens TIM Trio whole-body scanner located in the Hospital of the University of Pennsylvania. Signal excitation and reception were obtained using a quadrature body coil for transmit and a 32-channel head coil for receive. Gradient performance was 45 mT/m, with a maximum slew rate of 200 T/m/s. Image processing and analysis were performed using AFNI, FSL, and DTI specific tools with the advanced neuroimaging tools (ANTs) pipeline (Avants et al. 2011a,b).

Structural

Parameters of brain anatomy were derived from volumetric scans (T1-weighted) and DTI.

Volumetric MRI. Brain volumetric imaging was obtained using a magnetization prepared, rapid-acquisition gradient-echo (MPRAGE) sequence (TR/TE/TI = 1810/3.5/1100 ms; FOV RL/AP = 180/240 mm; Matrix RL/AP/slices = 192/256/160 Slice thick/gap = 1/0 mm; Flip angle = 90; No Reps; GRAPPA factor = 2; BW/pixel = 130 Hz; PE direction = RL; Acq time = 3:28 min). Receive coil shading was reduced by selecting the Siemens prescan normalize option, which is based on a body coil reference scan. Image quality assessment (QA) was performed both by visual inspection and with algorithms to detect artifacts such as related to excessive head motion.

To maximize accuracy, advanced structural image processing, quality assurance, and registration procedures were employed for the measurement of the cortical subcortical and cerebellar volumes and GMD. Estimation of brain regions used a multiatlas labeling approach. A set of 24 young adult T1-weighted volumes from the OASIS dataset (Marcus et al. 2007) were manually labeled and registered to each subject's T1-weighted volume using the top-performing SyN diffeomorphic registration (Avants et al. 2011a; Klein et al. 2010). These label sets were synthesized into a final parcellation using joint label fusion, which is similarly reliable to other state-of-the-art label fusion algorithms but uses significantly fewer atlases, and is far more accurate than segmentation performed with a single atlas (Wang et al. 2013). Volume was determined for each parcel using the intersection between the parcel created and prior driven GM cortical segmentation from the ANTs cortical thickness

pipeline as described below. Density estimates were calculated within each parcel as described below. To avoid registration bias and maximize sensitivity to detect regional effects that can be impacted by registration error, a custom adolescent template and tissue priors were created using data from 140 PNC participants, balanced for age and sex. Structural images were then processed and registered to this custom template using the ANTs cortical thickness pipeline (Tustison et al. 2014). This procedure includes brain extraction, N4 bias field correction (Tustison et al. 2010), Atropos tissue segmentation (Avants et al. 2011b), and SyN diffeomorphic registration method (Avants et al. 2011a; Klein et al. 2010).

Finally, GMD was calculated using Atropos (Avants et al. 2011b), with an iterative segmentation procedure that is initialized using 3-class K-means segmentation. This procedure produces both a discrete 3-class hard segmentation as well as a probabilistic GMD map (soft segmentation) for each subject. GMD was calculated within the intersection of this 3-class segmentation and the subject's volumetric parcellation (Gennatas et al. 2017). Images included in the final analysis passed a rigorous QA procedure, including evaluation of motion, as previously detailed (Rosen et al. 2018).

Diffusion (DTI). Diffusion weighted imaging (DWI) scans for measuring water diffusion were obtained using a twice-refocused spin-echo single-shot EPI sequence. The sequence employs a 4-lobed diffusion encoding gradient scheme combined with a 90–180-180 spin-echo sequence designed to minimize eddy-current artifacts. The sequence consisted of 64 diffusion-weighted directions with $b = 1000$ s/mm^2, and 7 scans with $b = 0$ s/mm^2.

Diffusion data were skull stripped by generating a brain mask for each subject by registering a binary mask of a standard image (FMRIB58_FA) to each subject's brain using FLIRT (Jenkinson et al. 2002). When necessary, manual adjustments were made to this mask. Next, eddy currents and movement were estimated and corrected using FSL's eddy tool (Andersson and Sotiropoulos, 2016; Graham et al. 2016; Roalf et al. 2016). Eddy improves upon FSL's Diffusion Tool Box (Behrens et al. 2003) and eddy correct tool (Andersson and Sotiropoulos 2016; Graham et al. 2016) by simultaneously modeling the effects of diffusion eddy current and head movement on DTI images, reducing the amount of resampling. The diffusion gradient vectors were rotated to adjust for motion using the 6-parameter motion output generated from the eddy. Then, the B0 field map was estimated and distortion correction was applied to the DTI data using FSL's FUGUE (Smith 2002). Finally, the diffusion tensor was modeled and metrics (MD) were estimated at each voxel using FSL's DTIFIT.

Registration from native space to a template space was completed using DTI-TK (Zhang et al. 2014; Zhang and Laidlaw 2006). First, DTI output files from DTIFIT were converted to DTI-TK format. Next, a template was generated from the tensor volumes using 14 representative diffusion datasets that were considered "Excellent" from the PNC sample. One individual from each of the 14 ages (age range 8–21) was randomly selected. These 14 DTI volumes were averaged to create an initial template. Next, data from the 14 subjects were registered to this template in an iterative manner. Unlike standard intensity-based registration algorithms, this process utilizes the full tensor information to best align the underlying WM tracts using iterations of rigid, affine, and diffeomorphic registration leading to the generation of a successively refined template. Ultimately, one high-resolution refined template was created and used for registration of the remaining diffusion datasets. All DTI maps were then registered (rigid, affine, diffeomorphic) to the high-resolution study-specific template using DTI-TK. Whole-brain analysis was performed using a customized implementation of tract-based spatial statistics (Bach et al. 2014). MD values were computed using a study-specific WM skeleton. MD has excellent intrasession and acceptable intersession reliability, especially for sequences with more gradient directions and repetitions within a session, as is the case in the present study (Wang et al. 2012). Then, standard regions of interest (ROI; ICBM-JHU WM Tracts; Harvard-Oxford Atlas) were registered from MNI152 space to the study-specific template using ANTs registration (Avants et al. 2011a). Mean diffusion metrics were extracted from these ROIs using FSL's "fslmeants." Images included in this final analysis passed a stringent QA procedure as previously detailed (Roalf et al. 2016).

Functional

Perfusion (ASL) measures of CBF. Brain perfusion was imaged using a pseudo continuous arterial spin labeling sequence (Wu and Wong, 2007), which has been shown to have good to excellent scan–rescan reliability within the site (Almeida et al. 2018). The sequence used a single-shot spin-echo EPI readout. Parallel acceleration (i.e., GRAPPA factor = 2) was used to reduce the minimum achievable echo time. The arterial spin labeling parameters were: label duration = 1500 ms, postlabel delay = 1200 ms, labeling plane = 90 mm inferior to the center slice. The sequence alternated between label and control acquisitions for a total of 80 acquired volumes (40 labels and 40 controls), the first being a label.

ASL data were preprocessed using standard tools included with FSL (Jenkinson et al. 2012). Following distortion correction using the B0 map with FUGUE, the first four image pairs were removed, the time series was realigned in MCFLIRT (Jenkinson et al. 2002), the skull was removed with BET (Smith 2002), and the image was smoothed at 6 mm FWHM using SUSAN (Smith and Brady 1997). CBF was quantified from control-label pairs using ASL Toolbox (Wang et al. 2008). As prior (Satterthwaite et al. 2014a), the T1 relaxation parameter was modeled on an age- and sex-specific basis (Wu et al. 2010). This model accounts for the fact that T1 relaxation time differs according to age and sex, and has been shown to enhance the accuracy and reliability of results in developmental samples (Jain et al. 2012). The CBF image was coregistered to the T1 image using boundary-based registration (Greve and Fischl 2009), and regional CBF values were averaged within each parcel. Subjects included in this analysis had low motion as measured by mean relative framewise displacement less than 0.5 mm.

Resting-state BOLD. Resting-state BOLD scans were acquired with a single-shot, interleaved multislice, gradient-echo, echo planar imaging (GE-EPI) sequence. In order to reach steady-state signal levels, the sequence performed two additional dummy scans at the start. The imaging volume was sufficient to cover the entire cerebrum of all subjects, starting superiorly at the apex. In some subjects, the inferior portion of the cerebellum could not be completely included within the imaging volume. The selection of imaging parameters was driven by the goal of achieving whole-brain coverage with acceptable image repetition time (i.e., TR = 3000 ms). A voxel resolution of $3 \times 3 \times 3$ mm with 46 slices was the highest obtainable resolution that satisfied those constraints (multiband acquisition methods were not available when these data were collected). During the

resting-state scan, a fixation cross was displayed as images were acquired. Participants were instructed to stay awake, keep their eyes open, fixate on the displayed crosshair, and remain still. Resting-state scan duration was 6.2 min.

Task-related BOLD. Task-related modulations of BOLD were measured using two fMRI tasks, as described in Satterthwaite et al. (2014a). The Nback working memory task involved the presentation of complex geometric figures (fractals) for 500 ms, followed by a fixed interstimulus interval (ISI) of 2500 ms. This occurred under three conditions: 0-back, 1-back, and 2-back, producing different levels of working memory load. In the 0-back condition, participants responded with a button press to a specified target fractal. For the 1-back condition, participants responded if the current fractal was identical to the previous one; in the 2-back condition, participants responded if the current fractal was identical to the item presented two trials previously. Each condition consisted of a 20-trial block (60 s); each level was repeated over three blocks. The target–foil ratio was 1:3 in all blocks, with 45 targets and 135 foils overall. Visual instructions (9 s) preceded each block, informing the participant of the upcoming condition. The task included a total of 72 s of rest while a fixation crosshair was displayed, which was distributed equally in three blocks of 24 s at beginning, middle, and end of the task. Total task duration was 11.6 min. The emotion identification (IdEmo) task employed a fast event-related design with a jittered ISI. Participants viewed 60 faces displaying neutral, happy, sad, angry, or fearful expressions, and were asked to label the emotion displayed. Each face was displayed for 5.5 s followed by a variable ISI of 0.5 to 18.5 s, during which a complex crosshair (that matched the faces' perceptual qualities) was displayed. Total IdEmo task duration was 10.5 min.

BOLD processing. Both task-related and resting-state task-free functional images were processed using a top-performing pipeline for removal of motion-related artifact (Ciric et al. 2017). Preprocessing steps included 1) correction for distortions induced by magnetic field inhomogeneities using FSL's FUGUE utility, 2) removal of the 4 initial volumes of each acquisition, 3) realignment of all volumes to a selected reference volume using MCFLIRT (Jenkinson et al. 2002), 4) removal of and interpolation over intensity outliers in each voxel's time series using AFNI's 3DDESPIKE utility (Cox 1996), 5) demeaning and removal of any linear or quadratic trends, and 6) coregistration of functional data to the high-resolution structural image using boundary-based registration (Greve and Fischl 2009). The artifactual variance in the data was modeled using a total of 36 parameters, including the 6 framewise estimates of motion, the mean signal extracted from eroded WM and cerebrospinal fluid compartments, the mean signal extracted from the entire brain, the derivatives of each of these 9 parameters, and quadratic terms of each of the 9 parameters and their derivatives. Both the BOLD-weighted time series and the artifactual model time series were temporally filtered using a first-order Butterworth filter with a passband between 0.01 and 0.08 Hz.

Subject exclusions were based on BOLD sequence specific quality control assessment. These included: lack of complete fMRI data for a particular task; high in-scanner motion (mean relative displacement > 0.5 mm or maximum relative displacement > 6 mm); poor brain coverage in fMRI data; or failure to perform tasks at a minimal level (N-back: more than 8 [>2 SD] nonresponses on the 0-back; emotion Identification: more than 11 [>2 SD] nonresponses, or number correct not significantly above chance performance [<18]).

BOLD outcome measures. ALFF: functional connectivity among brain regions is primarily attributable to correlations among low-frequency fluctuations in regional activation patterns (Di et al. 2013). The ALFFs shows high scan–rescan reliability within a session, with ICCs centered at approximately 0.8 (Somandepalli et al. 2015). The voxelwise amplitude of low-frequency fluctuations (ALFF; Yang et al. 2007) was computed as the sum (discretised integral) over frequency bins in the low-frequency (0.01–0.08 Hz) band of the voxelwise power spectrum, computed using a Fourier transform of the time-domain of the voxelwise signal. ALFF was calculated on data smoothed in SUSAN using a Gaussian-weighted kernel with 6 mm FWHM (Smith and Brady 1997). ALFF was selected because it is a frequently used measure derived from fMRI (PubMed crossing of fMRI and ALFF yielded 597 publications https://www.ncbi.nlm.nih.gov/pmc/?term=ALFF+and+fmri retrieved 27 September 2020).

ReHo: voxelwise ReHo (Zang et al. 2004) is equivalent to Kendall's coefficient of concordance computed over the time series in each voxel's local neighborhood. ReHo can thus be used as an estimate of the homogeneity of each neighborhood's activation pattern. ReHo shows moderate scan–rescan reliability within a session, with ICCs centered at approximately 0.6 (Somandepalli et al. 2015). Because spatial smoothing intrinsically elevates ReHo estimates by elevating spatial autocorrelation, Kendall's W was computed only on unsmoothed data. Each voxel's neighborhood was defined to include the 26 voxels adjoining its faces, edges, and vertices. The voxelwise homogeneity map was subsequently smoothed using a Gaussian kernel with FWHM of 6 mm in SUSAN to improve the signal-to-noise ratio (Smith and Brady 1997). Finally, regional ReHo values were then averaged across the anatomically derived subject-specific segmentation. Participants included in this analysis had low motion with a mean relative frame wise displacement less than 2.5 mm. ReHo was selected because it is among the most frequently used measures derived from resting-state fMRI (PubMed crossing of fMRI and ReHo yielded 549 manuscripts https://www-ncbi-nlm-nih-gov.proxy.library.upenn.edu/pubmed/?term=reho+and+fmri retrieved 3 July 2020).

ALFF and ReHo reflect different aspects of regional neural activity. ALFF measures the total power of the BOLD signal within the low-frequency range, and is thus proportional to regional neural activity, while ReHo is a voxel-based measure of the similarity between the time-series of a given voxel and its nearest neighbors, reflecting the synchrony of adjacent regions (see Lv et al. 2018; Zang et al. 2004).

Subject-level statistical analyses were carried out voxelwise with a canonical hemodynamic response function in FSL FEAT. For the n-back, 3 condition blocks (0-back, 1-back, and 2-back) were modeled. Six motion parameters and the instruction period were included as nuisance covariates, and the rest (fixation) condition provided unmodeled baseline. The dependent measure obtained was 2-back > 0-back, capturing the effect of increasing working memory load. For emotion identification, events were modeled as 5.5 s boxcar, matching the duration of face presentation. Five individual emotion regressors were included together with their temporal derivatives and six motion parameters. The contrast of interest was emotion face (happy+sad+anger + fear+neutral> fixation). Target ROIs for an NBack and an emotion identification task have acceptable reliability, as measured by relative agreement ICCs, over the course of 2 weeks (Plichta et al. 2012; but see Elliott et al. 2020).

Statistical Analysis

We examined the association of variability in brain structural and functional parameters and our performance parameter in four stages, aimed to contain type I error: 1) global values were examined for association with performance; 2) hypothesis testing, specifically the PFIT regions were examined across modalities compared with non-PFIT counterparts; 3) exploratory (hypothesis-generation), all regions were included and non-PFIT regions showing comparable significance and effect sizes were considered for inclusion in an Extended-PFIT (ExtPFIT) network; 4) data-driven performance prediction to estimate variance explained by brain parameters. Prior to further analyses, we compared correlations between performance and brain parameters in the left and right hemispheres and found that the effect sizes separating high and low performers were nearly identical in the two hemispheres for given regions, with left–right correlations ranging from the lowest of 0.833 for CBF to 0.944 for ReHo. Therefore, subsequent analyses summed or volume-averaged the two hemispheres as appropriate. Analyses were conducted using the open-source R platform (Version 3.5, R Core Team 2015).

Global values

The global measures included estimated total brain volume (TBV), average whole-brain values of GMD, MD, CBF, ALFF, ReHo, and the BOLD activation contrasts for the Nback and IdEmo tasks. The global measures were standardized within modality (Z-scores) prior to fitting the generalized estimating equations (GEEs) model. Since scaled total activation sums to zero, global values for the activation tasks were represented by activation their respective target regions, that is, midfrontal gyrus for the NBack and averaged activation in amygdala, anterior insula, and entorhinal cortex for the IdEmo. While analyzed as continuous variables, age interactions were visually examined by dividing the sample into children (ages less than 13), adolescents (ages 13–17), and young adults (ages 18 and older). Similarly, performance interactions were examined by dividing the sample into high, middle, and low-performance bins based on tertile splits of the age-regressed performance scores. These performance splits generated effect sizes by calculating the difference between the top performance tertile and the bottom performance tertile in standard deviation units (Cohen's D). This method of exploring higher-order interactions by examining not just *P*-values but also effect sizes were preferred over one that is guided by *P*-values alone as more reliable and interpretable (Kraemer 2019).

Hypothesis-testing

Regional analyses: testing PFIT. To test the PFIT, we examined regional specificity and compared regional differences of interactions with performance, contrasting PFIT with non-PFIT regions. GEEs models were fit within each modality. To minimize type I error given the large number of regions (up to 128 regions per modality), we aggregated them into 8 neuroanatomic sections: Fro, Tmp, Par, Occ, limbic (Lim), baso-striatal, cerebellum, and WM. The PFIT contrast was performed in sections that contained PFIT regions. Section volumes were derived using the sum of all regions involved, for all other brain measures a volume-weighted mean of the regions involved was calculated at the subject-level for each brain section.

For the hypothesis-testing approach, analyses were conducted at the global and regional levels by fitting GEEs with unstructured working correlation structure. GEE models are an extension of generalized linear models that estimate dependence among repeated measures by a user-specified working correlation matrix that allows for correlations in the dependent variable across observations. Five nested forms of GEE models were fit and evaluated as shown below. The null model (Model 1) evaluated the association of the demographic variables, age, and sex, on brain parameters. A second model added the performance term to evaluate the association between performance and brain parameters adjusted for demographic variables (Model 2). To evaluate if association of performance and brain parameters differed by sex or by age, interaction terms were added as shown in Model 3 and Model 4, respectively. To evaluate if association of performance and brain differed by both age and sex, Model 5 included all main effects and all possible interactions. Model performance was compared using a Wald test. A squared age term was included to capture nonlinear effects of age. Models were fit at all anatomical specificity levels. The hypothesis, PFIT, was tested by contrasting PFIT to non-PFIT regions across the brain with interaction analyses. This analysis was followed by examining the full model, which included brain region as a vector nested within each section.

Model 1: null model: sex and age associations:

$$\begin{aligned} Y_{ij} \;=\; & \beta_0 + \beta_1\left(\mathrm{Brain}_{ij}\right) + \beta_2\left(\mathrm{Sex}_i\right) + \beta_3\left(\mathrm{Age}_i\right) \\ & + \beta_4\left(\mathrm{Brain}_{ij} \times \mathrm{Sex}_i\right) + \beta_5\left(\mathrm{Brain}_{ij} \times \mathrm{Age}_i\right) \\ & + \beta_5\left(\mathrm{Sex}_i \times \mathrm{Age}_i\right) + \beta_6\left(\mathrm{Brain}_{ij} \times \mathrm{Sex}_i \times \mathrm{Age}_i\right) + \varepsilon_{ij} \end{aligned}$$

Model 2: model associations of performance and brain:

$$\begin{aligned} Y_{ij} \;=\; & \beta_0 + \boldsymbol{\beta_1}\left(\boldsymbol{Performance}_i\right) + \beta_2\left(\mathrm{Brain}_{ij}\right) + \beta_3\left(\mathrm{Sex}_i\right) \\ & + \beta_4\left(\mathrm{Age}_i\right) + \boldsymbol{\beta_4}\left(\mathbf{Performance}_i \times \mathbf{Brain}_{ij}\right) \\ & + \beta_5\left(\mathrm{Brain}_{ij} \times \mathrm{Sex}_i\right) + \beta_6\left(\mathrm{Brain}_{ij} \times \mathrm{Age}_i\right) \\ & + \beta_7\left(\mathrm{Sex}_i \times \mathrm{Age}_i\right) + \beta_8\left(\mathrm{Brain}_{ij} \times \mathrm{Sex}_i \times \mathrm{Age}_i\right) + \varepsilon_{ij} \end{aligned}$$

Model 3: Model with sex modifying the associations of performance and brain:

$$\begin{aligned} Y_{ij} \;=\; & \beta_0 + \beta_1\left(\mathrm{Performance}_i\right) + \beta_2\left(\mathrm{Brain}_{ij}\right) + \beta_3\left(\mathrm{Sex}_i\right) \\ & + \beta_4\left(\mathrm{Age}_i\right) + \beta_4\left(\mathrm{Performance}_i \times \mathrm{Brain}_{ij}\right) \\ & + \boldsymbol{\beta_5}\ \left(\mathbf{Performance}_i \times \mathbf{Sex}_i\right) + \beta_6\left(\mathrm{Brain}_{ij} \times \mathrm{Sex}_i\right) \\ & + \beta_7\left(\mathrm{Brain}_{ij} \times \mathrm{Age}_i\right) + \beta_8\left(\mathrm{Sex}_i \times \mathrm{Age}_i\right) \\ & + \boldsymbol{\beta_9}\left(\mathbf{Performance}_i \times \mathbf{Brain}_{ij} \times \mathbf{Sex}_i\right) \\ & + \beta_{10}\left(\mathrm{Brain}_{ij} \times \mathrm{Sex}_i \times \mathrm{Age}_i\right) + \varepsilon_{ij} \end{aligned}$$

Model 4: Model with age modifying the associations of performance and brain:

$$\begin{aligned} Y_{ij} = {} & \beta_0 + \beta_1 (\text{Performance}_i) + \beta_2 \left(\text{Brain}_{ij}\right) + \beta_3 (\text{Sex}_i) \\ & + \beta_4 (\text{Age}_i) + \beta_4 \left(\text{Performance}_i \times \text{Brain}_{ij}\right) \\ & + \boldsymbol{\beta_5} \ (\mathbf{Performance_i} \times \mathbf{Age_i}) + \beta_6 \left(\text{Brain}_{ij} \times \text{Sex}_i\right) \\ & + \beta_7 \left(\text{Brain}_{ij} \times \text{Age}_i\right) + \beta_8 (\text{Sex}_i \times \text{Age}_i) \\ & + \boldsymbol{\beta_9} \left(\mathbf{Performance_i} \times \mathbf{Brain_{ij}} \times \mathbf{Age_i}\right) \\ & + \beta_{10} \left(\text{Brain}_{ij} \times \text{Sex}_i \text{ X Age}_i\right) + \varepsilon_{ij} \end{aligned}$$

Model 5: Model with age and sex modifying the associations of performance and brain

$$\begin{aligned} Y_{ij} = {} & \beta_0 + \beta_1 (\text{Performance}_i) + \beta_2 \left(\text{Brain}_{ij}\right) + \beta_3 (\text{Sex}_i) \\ & + \beta_4 (\text{Age}_i) + \beta_5 \left(\text{Performance}_i \times \text{Brain}_{ij}\right) \\ & + \beta_6 (\text{Performance}_i \times \text{Sex}_i) + \beta_7 \ (\text{Performance}_i \times \text{Age}_i) \\ & + \beta_8 \left(\text{Brain}_{ij} \times \text{Sex}_i\right) + \beta_9 \left(\text{Brain}_{ij} \times \text{Age}_i\right) \\ & + \beta_{10} (\text{Sex}_i \times \text{Age}_i) + \beta_{11} \left(\text{Performance}_i \times \text{Brain}_{ij} \times \text{Sex}_i\right) \\ & + \beta_{12} \left(\text{Performance}_i \times \text{Brain}_{ij} \times \text{Age}_i\right) \\ & + \beta_{13} \left(\text{Brain}_{ij} \times \text{Sex}_i \times \text{Age}_i\right) + \boldsymbol{\beta_{14}} (\mathbf{Performance_i} \\ & \times \mathbf{Brain_{ij}} \times \mathbf{Sex_i} \times \mathbf{Age_i}) + \varepsilon_{ij} \end{aligned}$$

For all models above, $_i$ indicates the participant number, $_j$ indexes the individual brain spatial location, and $_{ij}$ denotes the random error.

Exploratory hypothesis-generation analyses. The hypothesis-testing phase was followed by an exploratory hypothesis-generation phase, where we used both *P*-values and effect sizes (see Kraemer 2019) to guide the search for additional regions as candidates for the ExtPFIT network. Exploratory analyses to understand neurodevelopmental changes were conducted for those brain sections and in those modalities that showed significant interactions with performance. Significant effects and interactions of performance were elucidated by charting the brain parameter profiles of effect sizes (Cohen D) for the differences between the high and low performance (tertiles) groups. Regions were rank-ordered for each modality (volume, GMD, etc.) by the *P*-value of its association with performance and by the effect size separating high from low performance (both after adjusting for covariates including quality metrics and reversing the sign of the effect sizes for MD and CBF, where lower values were hypothesized for the high-performance group). The averaged cross-modality ranking was considered evidence of cross-modality relevance to cognitive performance. From each section containing PFIT regions, we included non-PFIT regions showing a cross-modality ranking comparable or exceeding that of the PFIT region as candidates for inclusion in ExtPFIT. Finally, we examined effect sizes for cerebellar and WM regions for which cross-modality data were available.

Data-driven performance-prediction analysis. The CNB-based complex cognition performance factor score (Moore et al. 2015) was predicted using each brain parameter by modality. Subjects included in this analysis passed all modality-specific inclusion criteria. Within each modality and then across all modalities, three sets of regressions were fit in training sets, and R^2s were estimated in the corresponding test sets: 1) performance was regressed on scaled age, age^2, and age^3, 2) performance was regressed on scaled brain features subject to a ridge penalty, and 3) performance was regressed on scaled age, age^2, age^3, and brain features, with only the brain features subject to the ridge penalty. In each of 10 000 iterations for each set of regressions, the sample was stratified based on performance using the "createFolds" function from the "caret" package (Kuhn et al. 2016) in R into equally sized training and testing sets. Within each training fold that utilized ridge regression, a model was built using the "glmnet" function in the "glmnet" package (Friedman et al. 2010; Hastie and Tibshirani, 2010). The chosen ridge regression penalty parameter minimized out-of-sample mean squared error, where each test set was a unique fifth of the training set for the main ridge regression. The unique variance that brain features can explain in cognition above and beyond age was estimated by taking the difference in the means of the out-of-sample R^2s from 1) and 3). To test if this difference was significant, differences in R^2s were calculated for each test set. The proportion of R^2s in 3) that were greater than 1) for each modality within each sex served as the initial estimates for the *P*-values, to which FDR correction was then applied to control for multiple comparisons.

Results

Global Values

The global values showed generally small intercorrelations in either males or females, except for high negative correlations (exceeding 0.7) between volume and MD and similarly high positive correlations between ALFF and ReHo (Table 1). The small but significant negative correlation between GMD and CBF, seen both in males and females, confirms that low CBF does not simply reflect low GMD (since CBF is higher in GM than in WM) and is therefore likely of physiological significance. Note that since each modality required specific QA metrics for inclusion, the sample sizes for each modality differed somewhat, and Supplementary Table S1 compares included and excluded groups on sex, age, and performance.

The GEE indicated that performance was significantly associated with whole-brain global measures across modalities and this association differed by sex and age (GEE, Wald $\chi^2 = 59.51$, df = 30, $P = 0.001$). This interaction (Fig. 1) indicated that while high performers had higher volume and greater GMD compared with medium and low-performance groups, they had lower MD and CBF, no differences in ALFF, ReHo or the emotion identification task, and greater activation for the NBack task (first and third rows of Fig. 1). Global effect sizes of differences between performance groups became stronger from childhood to adulthood for volume and GMD as well as for NBack activation. For the other parameters, this trend seemed more pronounced in males than in females (second and fourth rows in Fig. 1).

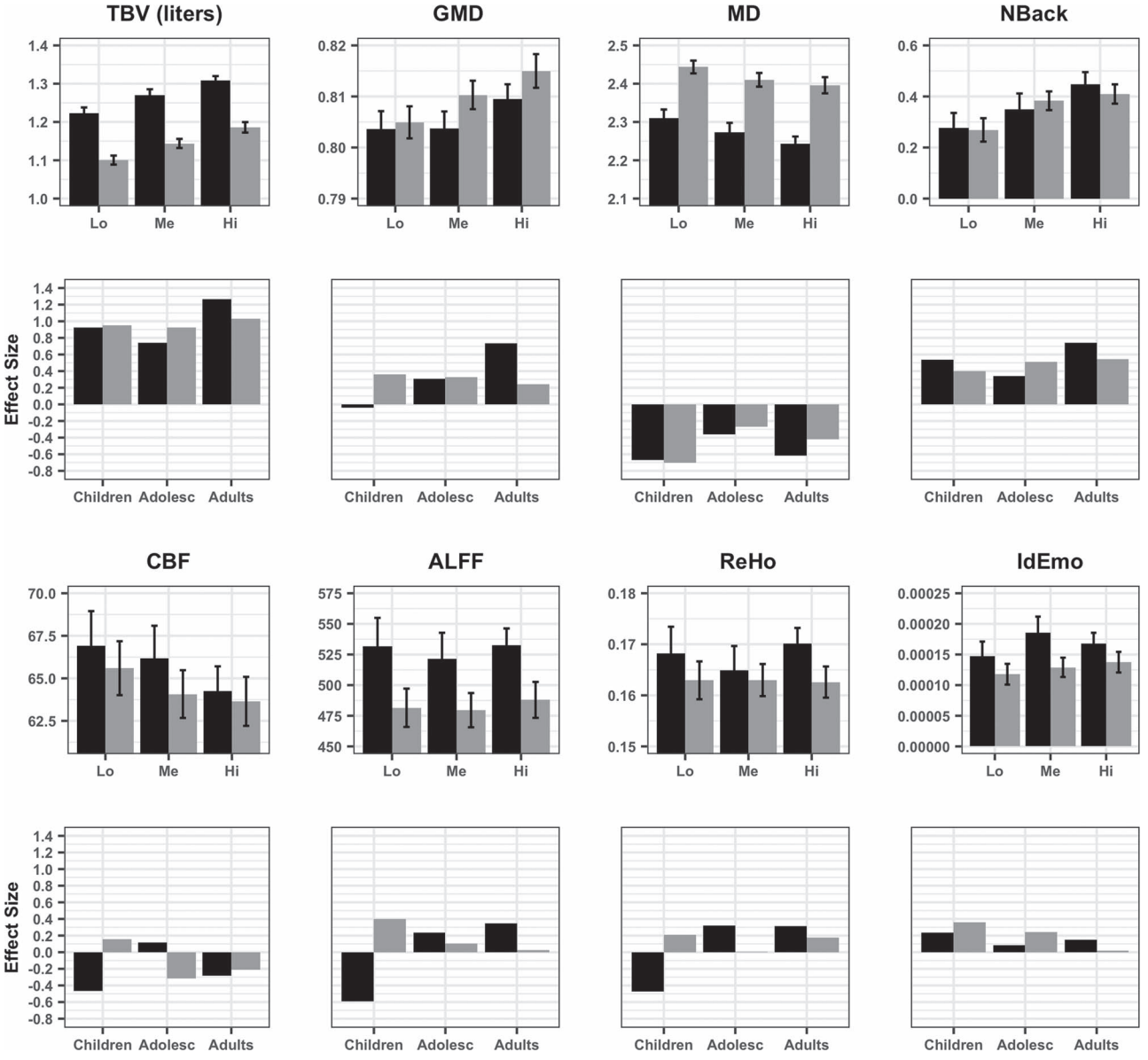

Figure 1. Global values for each modality by performance group (tertiles) in males (black) and females (gray). The first and third panels display means (±95% CI) of low (Lo), medium (Me), and high (Hi) tertiles of performers on volume, GMD, MD, CBF, ALFF, ReHo, NBack (Medial Frontal Gyrus), and IdEmo (Anterior Insula, Amygdala, Entorhinal Area). The second and fourth panels display effect sizes (Cohen's D) for the differences between high and low performers on each parameter in children, adolescents, and young adults. All figures were made using the R package "ggplot2" (Wickham, 2011).

Hypothesis testing

The results of the GEE contrasting PFIT to non-PFIT regions are summarized in Table 2. GEEs showed that in all modalities there was a highly significant Performance*PFIT interaction, indicating that performance related to these parameters differently in PFIT and non-PFIT regions. Some higher-order interactions with sex and age were also significant in some modalities, and the 4-way (Performance*PFIT vs non-PFIT*Sex*Age^2) was significant for GMD. The PFIT regions (Basten et al. 2015) and their cross-modality rankings percentiles are illustrated in Figure 2. As can be seen, PFIT regions (blue shaded) generally showed above average or high cross-modality rankings, supporting the PFIT hypothesis.

Exploratory Analyses

The exploratory GEE model did not contrast PFIT to non-PFIT regions, but instead included the region as a within-group ("repeated measures") vector nested within each of

Table 2 Results of the GEE analysis contrasting PFIT to non-PFIT regions with performance, sex, age, age^2, and the appropriate quality assurance metric as independent vectors

		Volume		GMD		MD		CBF		ALFF		ReHo		Nback		Idemo	
	df	χ^2	P	χ^2	P	χ^2	P	χ^2	P	χ^2	P	χ^2	P	χ^2	P	χ^2	P
Perf	1	**109.0**	**0.0000**	**135.1**	**0.0000**	**45.6**	**0.0000**	**94.0**	**0.0000**	**4.8**	**0.0292**	**9.8**	**0.0017**	**6.9**	**0.0084**	2.6	0.1069
PFIT	1	**119729.0**	**0.0000**	**9037.3**	**0.0000**	0.3	0.6005	**14853.0**	**0.0000**	**4617.2**	**0.0000**	**7887.2**	**0.0000**	**1235.1**	**0.0000**	**3122.7**	**0.0000**
Sex	1	**547.0**	**0.0000**	**17.8**	**0.0000**	**349.8**	**0.0000**	**7.0**	**0.0106**	**43.9**	**0.0000**	**11.1**	**0.0009**	0.1	0.7307	**5.6**	**0.0182**
Age	1	**63.0**	**0.0000**	**211.1**	**0.0000**	**12.2**	**0.0005**	**141.0**	**0.0000**	**87.8**	**0.0000**	**153.2**	**0.0000**	0.1	0.7956	0.3	0.6182
Age2	1	1.0	0.3902	0.7	0.4065	**7.7**	**0.0055**	**32.0**	**0.0000**	0.8	0.3585	0.4	0.5137	0.1	0.7154	0.1	0.7061
QA	1	1.0	0.4591	**235.1**	**0.0000**	**4.6**	**0.0324**	2.0	0.1980	30	**0.0000**	**30.9**	**0.0000**	0.2	0.7001	**4.3**	**0.0389**
Perf*PFIT	1	**235.0**	**0.0000**	**5.7**	**0.0172**	**12.3**	**0.0004**	**44.0**	**0.0000**	**26.7**	**0.0000**	**24.6**	**0.0000**	**47.8**	**0.0000**	**33.5**	**0.0000**
Perf*Sex	1	1.0	0.2671	2.2	0.1394	**5.9**	**0.0149**	**11.0**	**0.0009**	0.2	0.6321	0.6	0.4432	0.8	0.3877	0.3	0.5640
PFIT*Sex	1	**465.0**	**0.0000**	**105.7**	**0.0000**	**279.0**	**0.0000**	**5.0**	**0.0328**	0.7	0.3903	**5.7**	**0.0166**	**5.9**	**0.0155**	0.3	0.5824
Perf*Age	1	4.0	0.0520	**4.1**	**0.0430**	0.1	0.7183	1.0	0.2236	0.1	0.7336	0.6	0.4405	0.1	0.8275	0.3	0.5724
Perf*Age2	1	0.0	0.5722	0.1	0.7103	0.1	0.8271	0.0	0.5546	1	0.3094	0.1	0.8194	2.7	0.1036	0.2	0.6596
PFIT*Age	1	1.0	0.2283	2.7	0.1002	**76.5**	**0.0000**	**88.0**	**0.0000**	**7.1**	**0.0079**	2	0.1600	3.3	0.0714	**17.5**	**0.0000**
PFIT*Age2	1	0.0	0.6158	3.8	0.0498	1.4	0.2349	3.0	0.0631	**11.4**	**0.0007**	0.4	0.5261	3.8	0.0522	0.5	0.4708
Sex*Age	1	**8.0**	**0.0060**	0.6	0.4386	**10.2**	**0.0014**	**25.0**	**0.0000**	0.1	0.7079	0.6	0.4357	0.0	0.8594	0.0	0.8325
Sex*Age2	1	**8.0**	**0.0047**	0.1	0.8067	2.0	0.1605	**5.0**	**0.0210**	0.2	0.6488	1.4	0.2310	1.5	0.2166	1.4	0.2426
Perf*PFIT*Sex	1	1.0	0.2788	3.4	0.0655	**8.5**	**0.0035**	**8.0**	**0.0037**	2.4	0.1198	0.6	0.4293	0.0	0.9731	2.3	0.1280
Perf*PFIT*Age	1	**5.0**	**0.0233**	**10.3**	**0.0013**	1.2	0.2730	0.0	0.7808	0.3	0.5755	0.4	0.5144	0.0	0.8422	0.3	0.6045
Perf*PFIT*Age2	1	0.0	0.8277	0.7	0.4171	0.5	0.4924	0.0	0.7909	0.7	0.4003	0.1	0.7038	**6.1**	**0.0133**	0.0	0.8360
Perf*Sex*Age	1	1.0	0.2730	0.4	0.5266	4.2	0.0396	0.0	0.4874	**8.6**	**0.0034**	3.5	0.0630	0.0	0.8607	0.2	0.6797
Perf*Sex*Age2	1	1.0	0.2310	0.5	0.4883	0.0	0.9979	3.0	0.1134	2.8	0.0942	1.6	0.2037	0.7	0.4164	1.3	0.2624
PFIT*Sex*Age	1	**6.0**	**0.0149**	**7.0**	**0.0081**	0.9	0.3549	**11.0**	**0.0010**	0.5	0.4995	0.3	0.5795	0.1	0.8055	**5.9**	**0.0150**
PFIT*Sex*Age2	1	**8.0**	**0.0044**	**13.0**	**0.0003**	1.7	0.1868	0.0	0.7436	0	0.8558	0	0.9393	0.4	0.5480	0.3	0.5795
Perf*PFIT*Sex*Age	1	1.0	0.3340	2.0	0.1598	2.3	0.1311	0.0	0.5492	1.6	0.2088	0	0.8712	0.0	0.8808	4.1	0.0440
Perf*PFIT*Sex*Age2	1	1.0	0.3957	**7.5**	**0.0061**	1.5	0.2226	0.0	0.5524	0.2	0.6527	0.3	0.5629	0.1	0.8123	0.1	0.7339

Note: Perf = performance score; PFIT = parieto-frontal integration theory regions; QA = quality assurance metric; Bold = Significant; Bold Italics = Interacts with Performance; Italics = Marginally significant interaction with performance.

the 8 brain sections. All other effects (performance, sex, age, age^2, and QA metric) were the same, and we tested for all performance interactions in each of the 8 sections (Supplementary Table S2). The results showed highly significant (all $P < 0.001$) Performance*Region interactions in each and every modality for Fro, Tmp, and Par sections, and in all sections for volume, GMD and NBack. These interactions indicate regionally specific relations to performance in each brain section. Higher-order interactions involving age and sex were absent for volume but were highly significant in the other modalities, indicating that for brain parameters other than volume the relation between performance and brain parameters shows developmentally related sex differences.

To characterize the involvement of different parameters related to cognitive performance, we examined the cross-modality rankings in non-PFIT regions to identify candidates for inclusion in an ExtPFIT network—after controlling for age, sex, and scan quality (including motion). As can be seen in Figure 2, several regions were strong candidates for ExtPFIT (brown shaded) by showing performance-related cross-modality rankings that are comparable to those seen in PFIT regions. These results suggest that the PFIT should consider expansion to incorporate additional Fro (orbital, inferior and precentral, and mid superior Fro gyrus [SFG]), Tmp (temporal pole [TMP]) Par (supramarginal and angular gyri) and occipito-Tmp cortex (lingual and fusiform), as well as Lim (hippocampus [Hipp]) and baso-striatal (thalamus [Thal]) components.

To examine how these associations between brain parameters and performance are manifested in each modality and how they develop in males and females, we plotted effect sizes for PFIT and ExtPFIT regions. These results are detailed below.

Neuroanatomic parameters

The regional distribution of the PFIT and ExtPFIT effect sizes, contrasting high and low performers in children, adolescents, and young adults on each of the neuroanatomic parameters are shown in Figure 3.

As can be seen in Figure 3, for volume (upper row) all PFIT regions show moderate to large effect sizes indicating higher volumes in the high-performance groups across age groups and in both males and females. This effect increased linearly with advanced age in all regions for males, although there are several PFIT regions where children and adults have larger effect sizes than adolescents, while in females the effect reached adult size already during childhood in some regions. Several ExtPFIT regions showed comparable effect sizes (Fig. 3, upper row, regions under "Ext"), and they include the nucleus accumbens (NA) and Thal, implicating reward and relay system components in complex cognition. The Hipp is a Lim region that showed similar effect sizes as the anterior and posterior cingulate, the only Lim regions thus far implicated by PFIT (Basten et al. 2015). Similarly, superior, midfrontal, and somatomotor cortex were the only Fro regions included in PFIT, while our results indicate equal or higher effect sizes for the medial SFG and orbital (both inferior and posterior) cortex. Of the Tmp lobe regions, in addition to inferior, superior, and midtemporal regions, the TMP showed robust effect sizes, and for Par regions, the angular and supramarginal gyri showed similar effect sizes to the PFIT precuneus (PCu) and the SPL. Finally, the Occ fusiform cortex showed effect sizes similar and even exceeding the PFIT midoccipital region.

For GMD, we observed considerably smaller effect sizes compared with volume (Fig. 3, middle row). For PFIT relative to non-PFIT regions, this association differed by sex and by age^2 (Table 2), and this was the case for the Fro, Par, and Occ

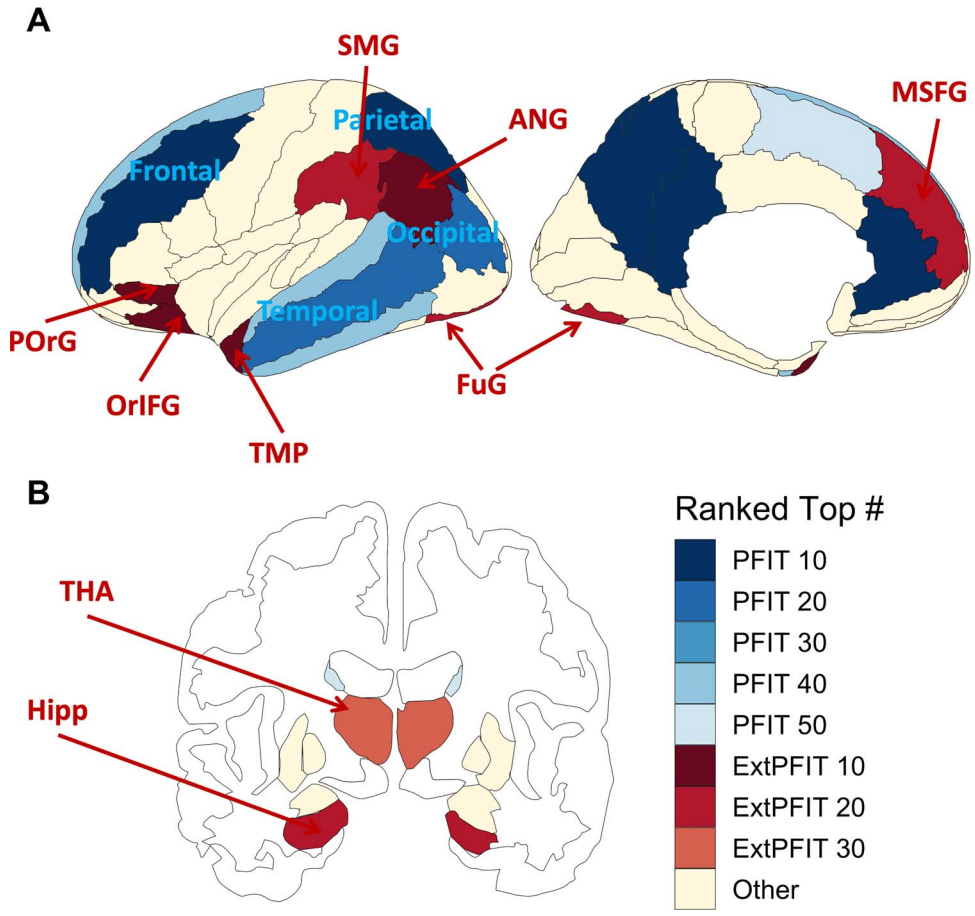

Figure 2. The image displays the number of modalities that ranked at the top when averaging P-value and effect sizes, colored by PFIT status (Statistical Analysis, third section). PFIT regions are in shades of blue, and extended-PFIT (ExtPFIT) regions are in shades of red. The P-values and effect sizes are for the performance predicting the normalized brain feature, controlling for normalized quality, age, age squared, and age cubed. Quality metrics are as follows: volume and GMD use the average manual rating; MD uses the temporal signal to noise ratio; and CBF, ALFFs, ReHo, NBack, and IdEmo use the mean of the relative root mean square displacements. This figure was made using the R package "ggseg" (Mowinckel and Vidal-Piñeiro, 2019).

lobes (Supplementary Table S2). High performers had higher GMD in PFIT regions across age and sex groups, except for male children, and in males, the effect sizes increased in most regions from childhood (negative) to adolescence to young adulthood (positive), while in females they remained generally stable across age bins. ExtPFIT regions (Fig. 3, middle row, regions under "Ext") likewise showed small to moderate effect sizes in the direction of higher values in the high-performance group, with the largest effects in the adult males. The ExtPFIT regions did not differ in performance group effects from the original PFIT regions.

MD showed much larger effect sizes than GMD in the direction of lower values in high performers compared with low performers (Fig. 3, lower row). Indeed, these effect sizes approached those for volume in Fro, Tmp, and Occ PFIT regions, although not in Par PFIT regions. These effects appeared across age groups but became most pronounced with advanced developmental age, especially in males. For the Par component of PFIT, this effect was seen only in the SPL and not in PCu, and the effects on Lim components of PFIT were in the opposite direction. Several ExtPFIT regions, specifically Fro and Par, showed similar effect sizes in the same direction, and the effect is evident in ExtPFIT Par regions, where it was absent in PFIT Par regions.

Neurophysiologic parameters

Effect sizes for the neurophysiologic parameters are shown in Figure 4. For CBF (Fig. 4, top row), PFIT regions showed small to moderate effect sizes, some reaching −0.5 SDs, of lower CBF associated with high performance. These associations were stronger for males than females and showed bigger increase from adolescence to young adulthood in males. Several ExtPFIT regions showed similar effect sizes in the same direction, including baso-striatal (NA and Thal) and Lim (Hipp) regions.

For ALFF (Fig. 4, middle row), high performers had higher values in most PFIT regions and across age groups with small to moderate effect sizes (0.2 to 0.5 SDs), with the exception of male children who showed moderate to large effect sizes (up to −0.9 SDs) in the opposite direction. Similar effects were seen in most ExtPFIT regions. Effect sizes for ReHo (Fig. 4, bottom row) were of similar direction and magnitude to those for ALFF.

Effect sizes for the activated fMRI are presented in Figure 5. The results for the working memory (NBack) task (upper row) give remarkably strong support for the narrow PFIT model, as moderate to large effect sizes are seen across the age groups for Fro and Par regions from the original PFIT. Notably, the Thal,

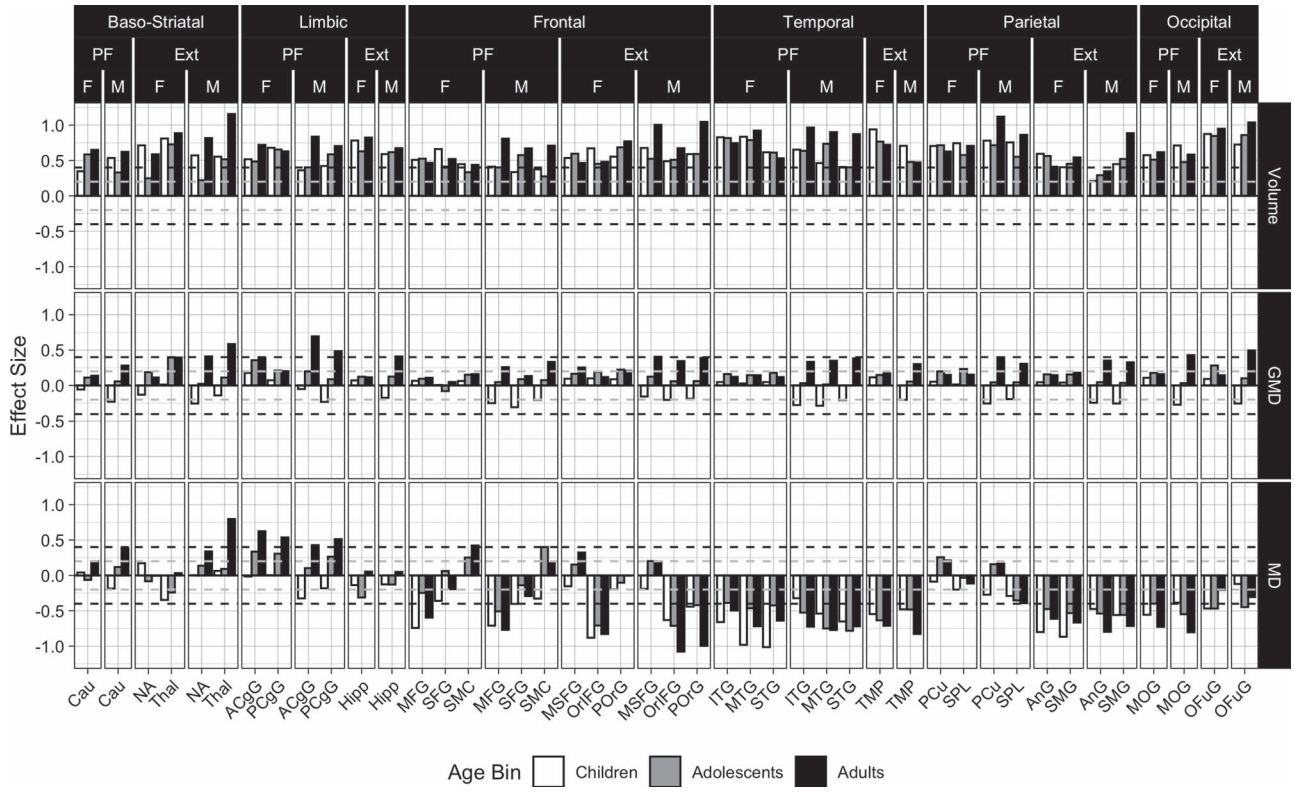

Figure 3. Developmental and sex effects for the association between structural brain features and high versus low performers are displayed. Effects shown are for volume (upper panel), GMD (middle panel), and MD (lower panel). Females (F) and males (M) are in white (children), gray (adolescents), and black (adults). Effect sizes are the coefficients for the indicator variable for the high compared with low performers predicting the scaled brain feature, controlling for scaled quality, age, age squared, and age cubed within each age bin. The quality metric for volume and GMD is the average manual rating, and for MD is the Tmp signal to noise ratio. The subset of non-PFIT regions that rank at or above PFIT regions, and therefore are considered for the ExtPFIT, are also displayed. Horizontal dashed lines indicate the transition from small to moderate effect sizes. Regional abbreviations: Cau = caudate nucleus; ACgG = anterior cingulate gyrus; PCgG = posterior cingulate gyrus; MFG = middle frontal gyrus; SMC = supplementary motor cortex; MSFG = superior frontal gyrus medial segment; OrIFG = orbital part of the inferior frontal gyrus; POrG = posterior orbital gyrus; ITG = inferior temporal gyrus; MTG = middle temporal gyrus; STG = superior temporal gyrus; AnG = angular gyrus; SMG = supramarginal gyrus; MOG = middle occipital gyrus; OFuG = occipital fusiform gyrus.

from the ExtPFIT, shows a similar effect size, supporting its role in cognition. In contrast to the NBack, effect sizes are generally negligible to small for the emotion identification task (Fig. 5, lower row).

Cerebellum and WM. As can be seen in Fig. 6, moderate to large effect sizes separating high and low performers were seen for volume in some cerebellar regions and all WM regions. These effect sizes were seen in all age groups but were most pronounced in the oldest group of young adult males, where they reached and sometimes exceeded 1SD. For WM, MD, and CBF showed small to moderate effects in the direction of lower values associated with better performance. The cerebellar regions showing the most robust effect sizes were lobules 8–10 and exterior cerebellum. Effect sizes in other modalities measured were small to moderate; they are shown for future reference and will not be further discussed.

Data-Driven Analyses

Each modality considered alone explained at least 9% of the variance in performance, estimated out-of-sample, with volume explaining the greatest proportion of the variance for both females and males (31.9 and 32.1%, respectively). However, since in this age range of 8–22 years both performance and brain parameters are highly correlated with age, we aimed to establish how much variance in performance is explained by brain parameters above and beyond age. We found that volume, GMD, NBack activation, and all of the modalities combined explained a significant amount of variance in cognition above and beyond the age for females, while the only volume did so for males (Fig. 7).

Discussion

Our results offer fresh insights regarding how cognition is related to multimodal parameters of brain structure and function. Global values for anatomic and physiologic parameters were associated with performance in modality-specific ways. Overall, high cognitive performers had anatomically higher volumes, higher GMD and lower MD, and physiologically they evinced lower CBF and higher activation to the NBack task. In all those modalities, the age effects were significant and effect sizes separating high from low performers generally increased with age. Performance associations with global ALFF and ReHo were more complex and differed between males and females. Regional analyses (see below) indicated more consistent effects in specific regions. The results of the global values indicate that the brain parameters examined relate meaningfully to

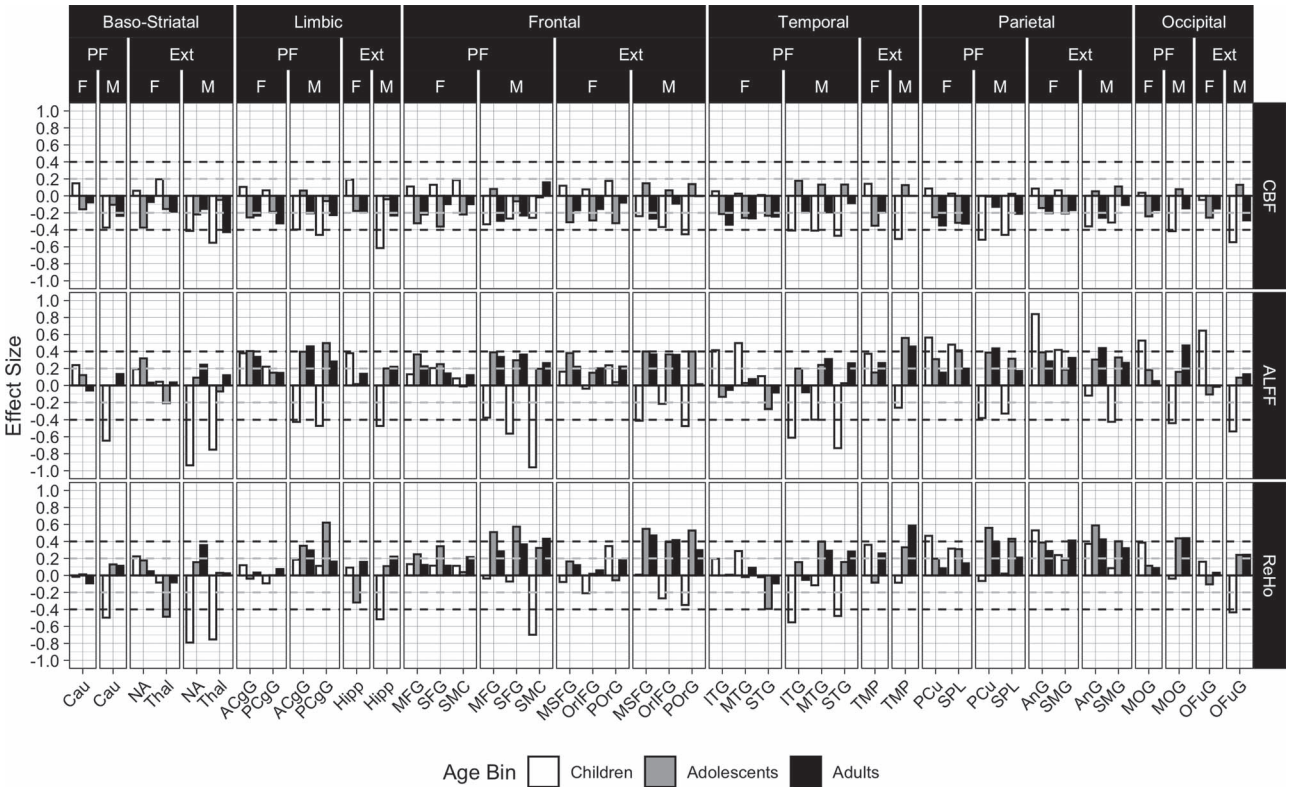

Figure 4. Developmental and sex effects for the association between functional brain features and high versus low performers are displayed. The quality metric for CBF, ALFFs, and ReHo is the mean of the relative root mean square displacements. All other values, legends, and abbreviations are as in Figure 3.

performance and that this relationship is strengthened during development.

The theoretical thrust of the analysis was to examine whether anatomic and physiologic indices derived from the network of regions included in PFIT indeed show association with cognitive performance, and whether other regions show similar performance associations warranting their inclusion in an ExtPFIT network. We found strong support for cross-modality involvement of PFIT regions, which showed significantly greater association with cognitive performance than non-PFIT regions in all modalities (see Table 2), and these relations were modulated only by age for volume and by higher-order interactions of age and sex for other parameters. Examination of effect sizes contrasting high and low performers indicated that they were large (up to >1 SDs for adult males, see Figure 3 top row) for higher volume and moderate for higher GMD, lower MD, lower CBF, higher ALFF, and ReHo, and greater activation to the NBack task. The amplitude and direction of results in this multimodal study are consistent with the literature and meta-analyses where subsets of these parameters have been examined in specific studies (Ritchie et al. 2015; Ryman et al. 2016; Gençet al. 2018; Yan et al. 2011; Hshieh et al. 2017; Rane et al. 2018; Pamplona et al. 2015; Vakhtin et al. 2014; Finn et al. 2015; Yoo et al. 2018; Fong et al. 2019; Greene et al. 2018, Dubois et al. 2018).

However, several regions not included in PFIT showed comparable cross-modality effect sizes and merited consideration for inclusion in an extended PFIT. These regions included some that surround the original PFIT regions, indicating that larger portions of Fro, Tmp, Par, and Occ cortex are involved in optimizing complex cognition. The Fro regions that should be considered for inclusion in ExtPFIT are adjacent to the PFIT but more posterior (somatosensory gyrus), medial (medial SFG), and inferior (orbital), suggesting the contribution of top–down regulatory systems for cognitive performance (Hampshire et al. 2010; Swick et al. 2008; Rolls and Grabenhorst 2008; Wojtasik et al. 2020). The Par candidates for ExtPFIT are the supramarginal and angular gyri, regions long implicated in complex cognition (Geschwind 1970; Tremblay and Dick 2016), as is the TMP, a region implicated in multimodal sensory integration (Olson et al. 2007) and social cognition (Pehrs et al. 2017), underscoring the role of Tmp lobe connectivity in complex cognition (Blazquez Freches et al. 2020). The Occ region that could be included in ExtPFIT, fusiform gyrus, is involved in high-order visual processing and would contribute visual memory and concept formation (Mechelli et al. 2000). In addition to these cortical areas, baso-striatal and Lim regions should be considered for ExtPFIT in addition to the caudate and cingulate included in the PFIT. The ExtPFIT seems to include the accumbens and Thal, reinforcing the striatal component that implicates motivational aspects of cognitive performance. Indeed, subcortical regions have been implicated in higher-order cognitive function and memory (Koziol et al. 2014; Münte et al. 2008; Wolff and Vann 2019), and ventral striatum activation signaling internal reward during NBack correlated with performance in the PNC (Satterthwaite et al. 2012). The Lim region added to the ExtPFIT model is the Hipp, implicating contributions of emotion regulation and episodic and contextual memory integration (Puigdemont et al. 2012, Aminoff et al. 2013). Thus, the original PFIT emphasized Fro and

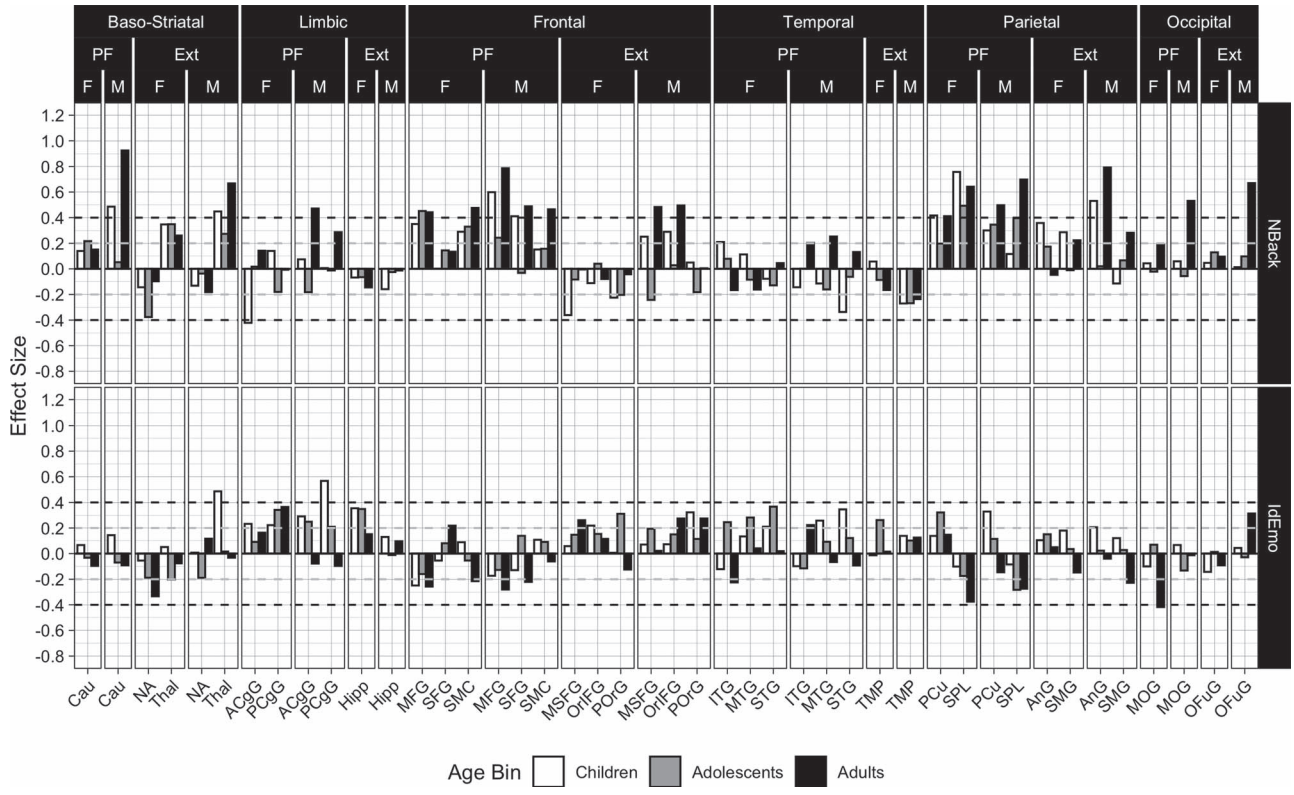

Figure 5. Developmental and sex effects for the association between performance (our main cognitive performance measure, which was obtained out of scanner) and activation on the NBack and IdEmo tasks in the same regions as in previous Figures. The quality metric for these effects is the mean of the relative root mean square displacements. All other values, legends, and abbreviations are as in Figure 3.

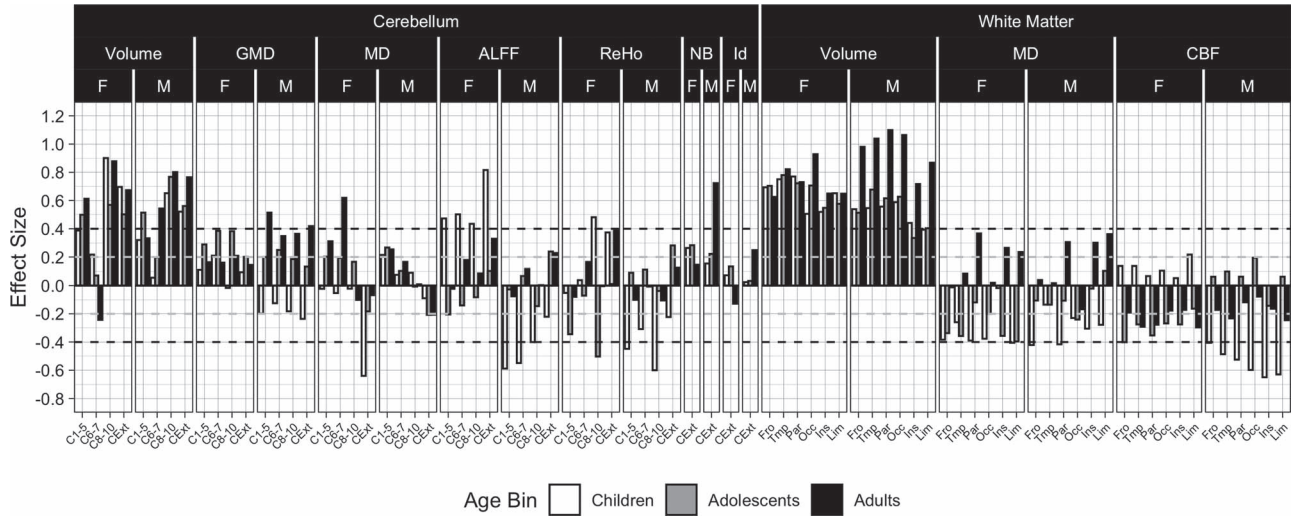

Figure 6. Developmental and sex effects for the association between performance and cerebellar and white matter features comparing high versus low performers. Quality metrics are as described for each modality in the above captions. Abbreviations: C1–5 = cerebellar layers I to V; C6–7 = cerebellar layers VI to VII; C8–10 = cerebellar layers VIII to X; CExt = cerebellar exterior; Ins = Insular. Other values and legends are as in Figure 3.

Par regions and subsequent meta-analyses implicated some additional Tmp, Occ, Lim, and striatal regions as important nodes of the complex cognition network. Our results from a multimodal study of a single large sample indicate that the network should be broadened, and optimal cognitive performance relates to a multimodal network with the robust representation of regions required for integrating conceptual processing with perception, memory, emotion regulation, and motivation.

Additional regions that show robust effect sizes related to performance were found in the cerebellum, specifically exterior and lobules 8–10. The cerebellum, traditionally considered

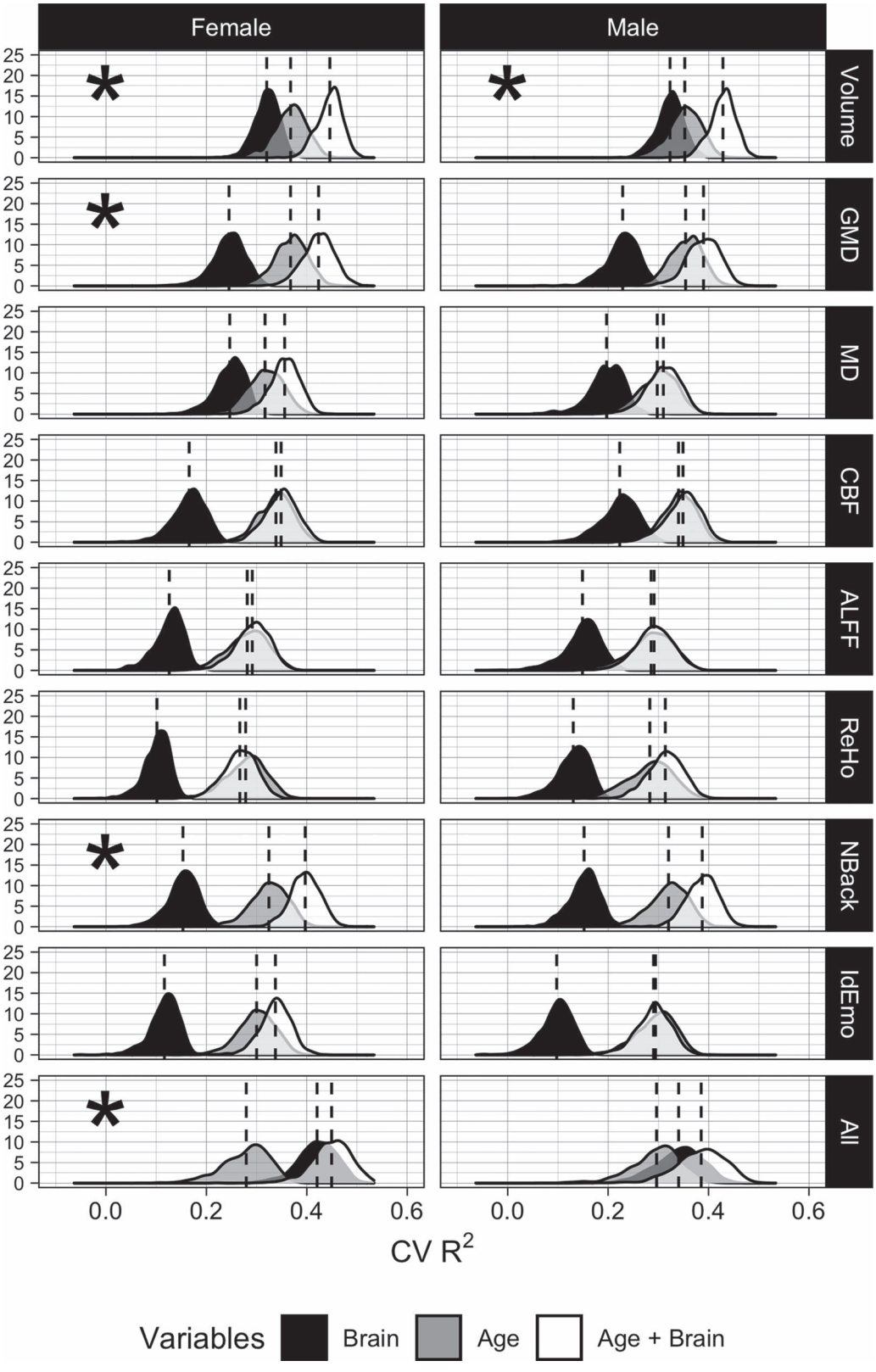

Figure 7. Results of ridge regressions predicting the executive functioning and complex cognition factor score for each modality and using all modalities ("All"). The distributions shown are out-of-sample R^2s over 10 000 iterations. For each R^2, a random half of the data was assigned to the training set, and the other half was assigned to the test set. R^2 was calculated using the following formula: $1 - {SS_{res}}/{SS_{tot}}$. The ridge hyperparameter lambda was chosen using 5-fold cross-validation on the training data. The lambda that minimized the out-of-sample MSE was selected. Asterisks indicate if adding the penalized brain features to the model with age explained significantly more variance in cognition than age alone.

primarily in relation to motor function and coordination, has been increasingly recognized as a hub related to cognition (Koziol et al. 2014) and these regions within the cerebellum have been specifically implicated in cognition (Tedesco et al. 2011). In addition, all WM regions showed sizable effect sizes, ranging from 0.4 to >1 SD, with better performance associated with higher volumes, as well as reduced MD and CBF. These findings indicate that WM integrity and tuning contribute to optimize cognitive performance.

The sample's age range from childhood to young adulthood allowed examination of developmental effects and sex differences in the magnitude of effect sizes related to performance. For volume, these effect sizes were stable across age groups, with a significant interaction with age showing that they tend to increase in size from childhood to adulthood. For the other modalities, the results showed higher-order interactions with age and sex, indicating that these parameters become optimized for performance over development at different rates in males and females. The sex differences overall seem to indicate complementary mechanisms in males and females that serve to compensate for sex differences across brain parameters. Sex differences in brain-behavior associations have been well documented (e.g., Goldstein et al 2001; Gur et al. 1982, 1999, 2000; Jazin and Cahill 2010; Ragland et al. 2000; Raznahan et al. 2011; Satterthwaite et al. 2015). Thus, lower volume in females is compensated for by higher GMD, and performance is further modulated by MD, CBF, ALFF, and ReHo, which may together account for equal cognitive performance. Furthermore, age-related differences in this developmental cohort were smaller for females than for males, indicating that females reach adult differences earlier, consistent with other studies (Erus et al. 2014; Goyal et al. 2019). We might speculate that earlier stabilization of metabolic parameters in females helps sustain brain integrity throughout the adult lifespan. Such complementarity between the sexes might have enhanced survival and reproduction in humans' environment of evolutionary adaptedness (Barkow et al. 1995). These sex differences could further reflect complementary reliance on different aspects of brain structure and function to optimize cognitive performance.

The data-driven analysis indicated that volume was far and away the brain parameter most strongly associated with cognitive performance, confirming earlier findings associating higher brain volumes with better cognitive abilities (Witelson et al. 2006; Gignac and Bates, 2017; Nave et al. 2019; Pietschnig et al. 2015). In our sample, effect sizes separating high from low-performance groups were moderate to large, and cross-validated R^2s for predicting performance based on volume alone exceeded 0.3 for both females and males (see Fig. 7). This estimate of explained variance is at the upper range of estimates from prior studies, which vary from 3% to >30%. Most previous studies to which we can compare our results examined volume. Our R^2 values are considerably higher than those reported for volumes by Nave et al. (2019), who estimate that volume explains slightly over 3% of the variance in cognitive performance in an adult sample (age range 40–69 years). Possibly the more extensive battery on which our performance measure was based, as well as the use of the same scanner, could have eliminated some sources of noise in estimating the dependent measures. We also established that high GMD relates to better performance, although the variance explained beyond age was more modest (5.58% of the variance for females and 3.56% for males). The other parameters showed smaller predictive power, except for the activation to the NBack task, which uniquely explained a substantial amount of out-of-scanner performance. These results are consistent with earlier work showing that task-activated fMRI is a better predictor of performance than resting-state measures (Greene et al. 2018; Yoo et al. 2018). Overall, considering the inherent error in all our measurements, these results indicate a substantial coupling between cognitive performance and parameters of brain structure and function.

It is notable that CBF was measured at a resting state, characterized as the "default mode" (Raichle et al., 2001) condition. Our finding that lower resting-state CBF is associated with better overall performance is consistent with reports that deactivation of the default-mode network during task performance is as predictive of performance as activation of task-related regions (Satterthwaite et al., 2013). A lower basal metabolic rate, as indicated by lower basal CBF, could be indicative of greater metabolic efficiency and potentially suggest a greater dynamic range in brain function. Thus, a lower "idling rate" may be conducive to better performance by permitting activation when the individual is faced with a task while preserving energy in the absence of a task.

Several limitations of this study are noteworthy. First and foremost, the study is cross-sectional and therefore unable to evaluate developmental trajectories of performance and brain parameters. All conclusions regarding age-related differences are limited by this feature of the data and longitudinal studies are needed to establish trajectories of the observed associations. The age range of the sample, 8–22 years, limits generalizability to other ages. Within this age range, in which age-related differences were seen in all brain modalities examined, the performance-related differences were generally consistent and replicated in all age groups. Another limitation of the study was the focus on a single parameter of cognitive capacity. This focus was necessitated by the complexity of probing multiple brain regions across modalities and accounting for age effects and sex differences. The measure selected is the closest proxy for "IQ," which was used in other studies and thus improves comparability of results. Future analyses can focus on other performance domains, such as episodic memory and social cognition, and more specific aspects of performance, such as accuracy compared with speed. The study is also limited by analyzing data across the entire sample, which is quite heterogeneous and, while ascertained through general pediatric services and not psychiatric services, still included individuals with significant psychopathology (Calkins et al. 2015) and adverse life events (Barzilay et al. 2019, 2020), and from diverse sociodemographic, ethnic and racial backgrounds. Perhaps stronger and more coherent effects could be seen if we limited the analyses to the subsample of typically developing youth without any significant disorder or to more homogeneous populations. We believe that while such analyses have merit and could reveal the effects of different disorders on the observed relationships, the heterogeneity and diversity of our sample enhance the generalizability of the reported results. Additionally, our analyses examined regional parameters of brain structure and function and related them to individual differences in behavioral measures of cognitive performance taken within the same timeframe, but not contemporaneously in the scanner. More variance in behavioral measures could be linked to functional brain parameters acquired contemporaneously (Roalf et al. 2014b). Finally, our analyses are limited by variability among parameters in the reliability of measures and by the high dimensionality of the data necessitating control for multiple comparisons. The reliability of the measures used in this study is acceptable to high, and

we have incorporated approaches to reduce data dimensionality and contain Type I error, but our approach may have obscured important findings that future work, better addressing these issues, can reveal.

Notwithstanding its limitations, the present study provides some "benchmarks" for assessing relations among brain parameters and performance. The results can guide hypotheses on how brain structure and function relate to individual differences in cognitive capacity, and offer the ability to gauge the relevance to cognitive performance of group differences or changes in brain parameters. Furthermore, acquisition of each parameter is costly in time and data management resources, and our study can inform the design of future large-scale neuroimaging studies based on the relevance of associating acquired brain parameters with cognitive performance. Since volume and GMD measures can be obtained rapidly and have shown the least susceptibility to QA failure in our data, they have key advantages in studies seeking to establish neural substrates of cognition. Activated fMRI can offer more specific associations to performance than resting-state physiologic measures, and multimodal collections including future efforts at multivariate integration across modalities could take advantage of their complementary strengths and weaknesses. Our finding of lower resting CBF in high performers is worthy of special emphasis since, unlike the structural parameters of volume, GMD, and MD, it relates to brain function. Uncovering a physiologic index associated with individual differences in cognitive performance has important implications for developing a scientific basis for social and medical prevention, education, and intervention strategies. Anatomy is unlikely to be readily affected by behavioral or pharmacologic treatment. By contrast, physiologic states such as measured by CBF, ALFF, ReHo, and BOLD activation, can be changed within seconds, and it is easier to conceive of treatments that can affect resting-state CBF for sustainable durations. Our results suggest questions for future investigation. For example, current methods for rehabilitation of brain dysfunction emphasize activation of task-related brain systems. Our findings that lower resting CBF and increased resting-state connectivity are associated with better performance suggest that emphasis should also be placed on training in the deactivation of task-relevant regions in the absence of a task. Indeed, our results may offer an avenue for future scientific probing of the benefits of procedures such as meditation, which emphasize relaxation associated with the absence of goal-oriented behavior and results in reduced default-mode activity (Brewer et al. 2011; Hasenkamp and Barsalou 2012). That both greater volume and GMD of brain and lower basal metabolic rate are associated with cognitive abilities is consistent with the preservation of tissue at low energy consumption as the "holy grail" for optimal organ function.

Supplementary Material

Supplementary material can be found at *Cerebral Cortex* online.

Author contributions

R.E.G. and R.C.G. conceived the project, designed the study, guided data analysis, interpreted the results, and wrote the manuscript. M.A.E., R.V., and J.A.D. designed the imaging protocol and participated in data analysis, R.C.G., E.R.B., T.M.M., A.F.G.R., A.P., and K.R. analyzed data, made figures and wrote sections of the manuscript. T.D.S., D.R.R., D.H.W., R.V., C.D., and E.D.G. guided image processing and interpretation of results. W.B.B. and R.T.S. guided statistical analysis. All authors reviewed and contributed to the write-up of the manuscript.

Notes

We thank the participants of the Philadelphia Neurodevelopmental Cohort and the members of the Recruitment, Assessment, Neuroimaging, and Data Teams whose contributions made this project possible. *Conflict of Interest:* None declared.

Funding

This work was supported by National Institutes of Health grant MH107235, MH089983, MH096891, MHP50MH06891, R01MH113550, R01MH112847, R01MH119219, the Dowshen Neuroscience fund, and the Lifespan Brain Institute of Children's Hospital of Philadelphia and Penn Medicine, University of Pennsylvania.

References

Almeida JR, Greenberg T, Lu H, Chase HW, Fournier JC, Cooper CM, Deckersbach T, Adams P, Carmody T, Fava M *et al.* 2018. Test-retest reliability of cerebral blood flow in healthy individuals using arterial spin labeling: findings from the EMBARC study. *Magn Reson Imaging*. 45:26–33.

Aminoff EM, Kveraga K, Bar M. 2013. The role of the parahippocampal cortex in cognition. *Trends Cogn Sci*. 17:379–390.

Andersson J and Sotiropoulos SN. 2016. An integrated approach to correction for off-resonance effects and subject movement in diffusion MR imaging. *NeuroImage*. 125:1063–1078.

Avants BB, Tustison NJ, Song G, Cook PA, Klein A, Gee JC. 2011a. A reproducible evaluation of ANTs similarity metric performance in brain image registration. *Neuroimage*. 54:2033–2044.

Avants BB, Tustiso NJ, Wu J, Cook PA, Gee JC. 2011b. An open source multivariate framework for n-tissue segmentation with evaluation on public data. *Neuroinformatics*. 9:381–400.

Bach M, Laun FB, Leemans A, Tax C, Biessels GJ, Stieltjes B, Maier-Hein KH. 2014. Methodological considerations on tract-based spatial statistics (TBSS). *Neuroimage*. 100:358–369.

Barkow JH, Cosmides L, Tooby J, editors. 1995. *The adapted mind: evolutionary psychology and the generation of culture*. New York, NY: Oxford University Press.

Barzilay R, Calkins ME, Moore TM, Wolf DH, Satterthwaite TD, Scott CJ, Jones JD, Benton TD, Gur RC, Gur RE. 2019. Association between traumatic stress load, psychopathology, and cognition in the Philadelphia neurodevelopmental cohort. *Psychol Med*. 49:325–334.

Barzilay R, White LK, Moore TM, Calkins ME, Taylor JH, Patrick A, Huque ZM, Young JF, Ruparel K, Pine DS *et al.* 2020. Association of anxiety phenotypes with risk of depression and suicidal ideation in community youth. *Depress Anxiety*. 10:1002.

Basten U, Hilger K, Fiebach CJ. 2015. Where smart brains are different: a quantitative meta-analysis of functional and structural brain imaging studies on intelligence. *Dermatol Int*. 51:10–27.

Behrens TE, Woolrich MW, Jenkinson M, Johansen-Berg H, Nunes RG, Clare S, Matthews PM, Brady JM, Smith SM. 2003. Characterization and propagation of uncertainty in diffusion-weighted MR imaging. *Magnetic resonance in medicine*. 50: 1077–1088.

Blazquez Freches G, Haak KV, Bryant KL, Schurz M, Beckmann CF, Mars RB. 2020. Principles of temporal association cortex organisation as revealed by connectivity gradients. *Brain Struct Funct*. 225:1245–1260.

Brewer JA, Worhunsky PD, Gray JR, Tang YY, Weber J, Kober H. 2011. Meditation experience is associated with differences in default mode network activity and connectivity. *Proc Natl Acad Sci USA*. 108:20254–20259.

Calkins ME, Merikangas KR, Moore TM, Burstein M, Behr A, Satterthwaite TD, Ruparel K, Wolf DH, Roalf DR, Mentch FD *et al*. 2015. The Philadelphia neurodevelopmental cohort: constructing a deep phenotyping collaborative. *J Child Psychol Psychiatry*. 56:356–1369.

Ciric R, Wolf DH, Power D, Roalf DR, Baum GL, Ruparel K, Shinohara RT, Elliott MA, Eickhoff S, Davatzikos C *et al*. 2017. Benchmarking of participant-level confound regression strategies for the control of motion artifact in studies of functional connectivity. *Neuroimage*. 154:174–187.

Cox RW. 1996. AFNI: software for analysis and visualization of functional magnetic resonance neuroimages. *Comput Biomed Res*. 29(3):162–173.

Di X, Kim EH, Huang CC, Lin CP, Biswal BB. 2013. The influence of the amplitude of low-frequency fluctuations on resting-state functional connectivity. *Front Hum Neurosci*. 7:118.

Dubois J, Galdi P, Paul LK, Adolphs R. 2018. A distributed brain network predicts general intelligence from resting-state human neuroimaging data. *Philos Trans R Soc Lond B Biol Sci*. 373(1756):1756–1768.

Elliott ML, Knodt AR, Ireland D, Morris ML, Poulton R, Ramrakha S, Sison ML, Moffitt TE, Caspi A, Hariri AR. 2020. What is the test-retest reliability of common task-functional MRI measures? New empirical evidence and a meta-analysis. *Biorxiv*. 2020. https://www.biorxiv.org/content/10.1101/681700v3 (last accessed, 26 September 2020).

Erus G, Battapady H, Satterthwaite TD, Hakonarson H, Gur RE, Davatzikos C, Gur RC. 2014. Imaging patterns of brain development and their relationship to cognition. *Cereb Cortex*. 25:1676–1684.

Estrada E, Ferrer E, Román FJ, Karama S, Colom R. 2019. Time-lagged associations between cognitive and cortical development from childhood to early adulthood. *Dev Psychol*. 55(6):1338–1352. doi: 10.1037/dev0000716.

Friedman J, Hastie T, Tibshirani R. 2010. Regularization paths for generalized linear models via coordinate descent. *Journal of Statistical Software*. 33:1–22.

Finn E, Shen X, Scheinost D, Rosenberg MD, Huang J, Chun MM, Papademetris X, Constable RT. 2015. Functional connectome fingerprinting: identifying individuals using patterns of brain connectivity. *Nat Neurosci*. 18:1664–1671.

Fong AHC, Yoo K, Rosenberg MD, Zhang S, Li CR, Scheinost D, Constable RT, Chun MM. 2019. Dynamic functional connectivity during task performance and rest predicts individual differences in attention across studies. *Neuroimage*. 188:14–25.

Genç E, Fraenz C, Schlüter C, Friedrich P, Hossiep R, Voelkle M, Ling JM, Güntürkün O, Jung RE. 2018. Diffusion markers of dendritic density and arborization in gray matter predict differences in intelligence. *Nat Commun*. 9: 1905.

Gennatas ED, Avants BB, Wolf DH, Satterthwaite TD, Ruparel K, Ciric R, Hakonarson H, Gur RE, Gur RC. 2017. Age-related effects and sex differences in gray matter density, volume, mass, and cortical thickness from childhood to young adulthood. *J Neurosci*. 37:5065–5073.

Geschwind N. 1970. The organization of language and the brain. *Science*. 170:940–944.

Gignac GE, Bates TC. 2017. Brain volume and intelligence: the moderating role of intelligence measurement quality. *Intelligence*. 64:18–29.

Goldstein JM, Seidman LJ, Horton NJ, Makris N, Kennedy DN, Caviness VS Jr, Faraone SV, Tsuang MT. 2001. Normal sexual dimorphism of the adult human brain assessed by in vivo magnetic resonance imaging. *Cereb Cortex*. 11: 490–497.

Goyal MS, Blazey TM, Su Y, Couture LE, Durbin TJ, Bateman RJ, Benzinge TL, Morris JC, Raichle ME, Vlassenko AG. 2019. Persistent metabolic youth in the aging female brain. *Proc Natl Acad Sci USA*. 116:3251–3255.

Greene AS, Gao S, Scheinost D, Constable RT. 2018. Task-induced brain state manipulation improves prediction of individual traits. *Nature commun*. 9:2807.

Greve DN, Fischl B. 2009. Accurate and robust brain image alignment using boundary-based registration. *Neuroimage*. 48:63–72.

Gur RC, Gur RE, Obrist WD, Hungerbuhler JP, Younkin D, Rosen AD, Skolnick BE, Reivich M. 1982. Sex and handedness differences in cerebral blood flow during rest and cognitive activity. *Science*. 217:659–661.

Gur RC, Turetsky BI, Matsui M, Yan M, Bilker W, Hughett P, Gur RE. 1999. Sex differences in brain gray and white matter in healthy young adults: correlations with cognitive performance. *J Neurosci*. 19:4065–4072.

Gur RC, Alsop D, Glahn D, Petty R, Swanson CL, Maldjian JA, Turetsky BI, Detre JA, Gee J, Gur RE. 2000. An fMRI study of sex differences in regional activation to a verbal and a spatial task. *Brain Lang*. 74:157–170.

Gur RC, Richard J, Hughett P, Calkins ME, Macy L, Bilker WB, Brensinger C, Gur RE. 2010. A cognitive neuroscience-based computerized battery for efficient measurement of individual differences: standardization and initial construct validation. *J Neurosci Methods*. 187:254–262.

Gur RC, Richard J, Calkins ME, Chiavacci R, Hansen JA, Bilker B, Loughead J, Connolly JJ, Qiu H, Mentch FD *et al*. 2012. Age group and sex differences in performance on a computerized neurocognitive battery in children age 8-21. *Neuropsychologia*. 26:251–265.

Gur RC, Calkins ME, Satterthwaite TD, Ruparel K, Bilker WB, Moore TM, Savitt AP, Hakonarson H, Gur RE. 2014. Neurocognitive growth charting in psychosis spectrum youths. *JAMA Psychiat*. 71:366–374.

Hampshire A, Chamberlain SR, Monti MM, Duncan J, Owen AM. 2010. The role of the right inferior frontal gyrus: inhibition and attentional control. *Neuroimage*. 50:1313–1319.

Hasenkamp W, Barsalou LW. 2012. Effects of meditation experience on functional connectivity of distributed brain networks. *Front Hum Neurosci*. 1:38.

Hilger K, Ekman M, Fiebach CJ, Basten U. 2017. Intelligence is associated with the modular structure of intrinsic brain networks. *Sci Rep*. 7(1):16088. doi: 10.1038/s41598-017-15795-7.

Hshieh TT, Dai W, Cavallari M, Guttmann CR, Meier DS, Schmitt EM, Dickerson C, Pres DZ, Marcantonio ER, Jones R *et al*. 2017. Cerebral blood flow MRI in the nondemented elderly is not predictive of post-operative delirium but is correlated with cognitive performance. *J Cereb Blood Flow Metab*. 37: 1386–1397.

Ingalhalikar M, Smit A, Parker D, Satterthwaite TD, Elliott MA, Ruparel K, Hakonarson H, Gur RE, Gur RC, Verma R. 2014. Sex differences in the structural connectome of the human brain. *Proc Natl Acad Sci USA*. 111:823–828.

Jain V, Duda J, Avants B, Giannetta M, Xie X, Roberts T, Detre JA, Hurt H, Wehrli FW, Wang DJJ. 2012. Longitudinal reproducibility and accuracy of pseudo-continuous arterial spin-labeled perfusion MR imaging in typically developing children. *Radiology*. 263:527–536.

Jangraw DC, Gonzalez-Castillo J, Handwerker DA, Ghane M, Rosenberg MD, Panwar P, Bandettini PA. 2018. A functional connectivity-based neuromarker of sustained attention generalizes to predict recall in a reading task. *Neuroimage*. 166:99–109.

Jazin E, Cahill L. 2010. Sex differences in molecular neuroscience: from fruit flies to humans. *Nat Rev Neurosci*. 11: 9–17.

Jenkinson M, Bannister P, Brady M, Smith S. 2002. Improved optimization for the robust and accurate linear registration and motion correction of brain images. *Neuroimage*. 17: 825–841.

Jenkinson M, Beckmann CF, Behrens TEJ, Woolrich MW, Smith SM. 2012. FSL. *Neuroimage*. 62:782–790.

Jung RE, Haier RJ. 2007. The Parieto-Frontal Integration Theory (P-FIT) of intelligence: converging neuroimaging evidence. *The Behavioral and Brain Sciences*. 30:135–187.

Klein A, Ghos SS, Avants B, Yeo BTT, Fischl B, Ardekani B, Gee JC, Mann JJ, Parsey RV. 2010. Evaluation of volume-based and surface-based brain image registration methods. *Neuroimage*. 51:214–220.

Koziol LF, Budding D, Andreasen N, D'Arrigo S, Bulgheroni S, Imamizu H, Ito M, Manto M, Marvel C, Parker K *et al*. 2014. Consensus paper: the cerebellum's role in movement and cognition. *Cerebellum*. 13:151–177.

Kraemer HC. 2019. Is it time to ban the P value? *JAMA Psychiat*. 76:1219–1220.

Kuhn M. 2016. contributions from Jed Wing. Weston, A. Williams, C. Keefer, A. Engelhardt, T. Cooper, Z. Mayer, B. Kenkel, the R Core Team, M. Benesty, R. Lescarbeau, A. Ziem, L. Scrucca, Y. Tang, and C. Candan., *Caret: classification and regression training*, 6–0.

Lv H, Wang Z, Tong E, Williams LM, Zaharchuk G, Zeineh M, Goldstein-Piekarski AN, Ball TM, Liao C, Wintermark M. 2018. Resting-state functional MRI: everything that nonexperts have always wanted to know. *Am J Neuroradiol*. doi: 10.3174/ajnr.A5527.

Marcus D, Wang TH, Parker J, Csernansky JG, Morris JC, Buckner RL. 2007. Open access series of imaging studies (OASIS): cross-sectional MRI data in young, middle aged, nondemented, and demented older adults. *J Cogn Neurosci*. 19:1498–1507.

Mechelli A, Humphreys GW, Mayall K, Olson A, Price CJ. 2000. Differential effects of word length and visual contrast in the fusiform and lingual gyri during reading. *Proc Biol Sci*. 267:1909–1913.

Moore TM, Reise SP, Gur RE, Hakonarson H, Gur RC. 2015. Psychometric properties of the Penn computerized neurocognitive battery. *Neuropsychologia*. 29:235–246.

Mowinckel AM, Vidal-Piñeiro D. 2019. Visualisation of brain statistics with r-packages ggseg and ggseg3d. arXiv preprint arXiv:1912.08200. https://arxiv.org/pdf/1912.08200.pdf.

Münte TF, Heldmann M, Hinrichs H, Marco-Pallares J, Krämer UM, Sturm V, Heinze HJ. 2008. Contribution of subcortical structures to cognition assessed with invasive electrophysiology in humans. *Front Neurosci*. 2:72–78.

Nave G, Jung WH, Karlsson Linnér R, Kable JW, Koellinger PD. 2019. Are bigger brains smarter? Evidence from a large-scale preregistered study. *Psychol Sci*. 30:43–54.

Pamplona GS, Santos Neto GS, Rosset SR, Rogers BP, Salmon CE. 2015. Analyzing the association between functional connectivity of the brain and intellectual performance. *Front Hum Neurosci*. 9:61.

Pehrs C, Zaki J, Schlochtermeier LH, Jacobs AM, Kuchinke L, Koelsch S. 2017. The temporal pole top-down modulates the ventral visual stream during social cognition. *Cereb Cortex*. 27:777–792.

Pietschnig J, Penke L, Wicherts JM, Zeiler M, Voracek M. 2015. Meta-analysis of associations between human brain volume and intelligence differences: how strong are they and what do they mean? *Neurosci Biobehav Rev*. 57:411–432.

Plichta MM, Schwarz AJ, Grimm O, Morgen K, Mier D, Haddad L, Gerdes AB, Sauer C, Tost H, Esslinger C *et al*. 2012. Test-retest reliability of evoked BOLD signals from a cognitive-emotive fMRI test battery. *Neuroimage*. 60:1746–1758.

Puigdemont D, Pérez-Egea R, Portella MJ, Molet J, de Diego-Adeliño J, Gironell A, Radua J, Gómez-Anson B, Rodríguez R, Serra M *et al*. 2012. Deep brain stimulation of the subcallosal cingulate gyrus: further evidence in treatment-resistant major depression. *Int J Neuropsychopharmacol*. 15:121–133.

Qiu D, Tan L-H, Zhou K, Khong PL. 2008. Diffusion tensor imaging of normal white matter maturation from late childhood to young adulthood: voxel-wise evaluation of mean diffusivity, fractional anisotropy, radial and axial diffusivities, and correlation with reading development. *Neuroimage*. 41:223–232.

Olson IR, Plotzker A, Ezzyat Y. 2007. The enigmatic temporal pole: a review of findings on social and emotional processing. *Brain*. 130:1718–1731.

R Core Team (2015). R foundation for statistical computing, Vienna, Austria. http://www.R-project.org/ (last accessed, 26 September 2020).

Raichle ME, MacLeod AM, Snyder AZ, Powers WJ, Gusnard DA, Shulman GL. 2001. A default mode of brain function. *Proc Natl Acad Sci USA*. 98:676–682.

Ragland JD, Coleman AR, Gur RC, Glahn DC, Gur RE. 2000. Sex differences in brain-behavior relationships between verbal episodic memory and resting regional cerebral blood flow. *Neuropsychologia*. 38:451–461.

Rane S, Koh N, Boord P, Madhyastha T, Askren MK, Jayadev S, Cholerton B, Larson E, Grabowski TJ. 2018. Quantitative cerebrovascular pathology in a community-based cohort of older adults. *Neurobiol Aging*. 65:77–85.

Raznahan A, Shaw P, Lalonde F, Stockman M, Wallace GL, Greenstein D, Clasen L, Gogtay N, Giedd JN. 2011. How does your cortex grow? *J Neurosci*. 31:7174–7177.

Ritchie SJ, Booth T, Valdés Hernández MD, Corley J, Maniega S, Gow AJ, Royle NA, Pattie A, Karama S, Starr JM *et al*. 2015. Beyond a bigger brain: multivariable structural brain imaging and intelligence. *Intelligence*. 51:47–56.

Roalf DR, Gur RE, Ruparel K, Calkins M, Satterthwaite TD, Bilker WB, Hakonarson H, Harris LJ, Gur RC. 2014a. Within-individual variability in neurocognitive performance: age- and sex-related differences in children and youths from ages 8 to 21. *Neuropsychologia*. 28:506–518.

Roalf DR, Ruparel K, Gur RE, Bilker W, Gerraty R, Elliott MA, Gallagher RS, Almasy L, Pogue-Geile MF, Prasad K *et al*. 2014b. Neuroimaging predictors of cognitive performance

across a standardized neurocognitive battery. *Neuropsychologia*. 28:161–176.

Rolls ET, Grabenhorst F. 2008. The orbitofrontal cortex and beyond: from affect to decision-making. *Prog Neurobiol*. 86:216–244.

Ryman SG, Yeo RA, Witkiewitz K, Vakhtin AA, van den Heuvel M, de Reus M, Flores RA, Wertz CR, Jung RE. 2016. Frontoparietal gray matter and white matter efficiency differentially predict intelligence in males and females. *Hum Brain Mapp*. 37:4006–4016.

Roalf DR, Quarmley M, Elliott MA, Satterthwaite TD, Vandekar SN, Ruparel K, Gennatas ED, Calkins ME, Moore TM, Hopson R *et al*. 2016. The impact of quality assurance assessment on diffusion tensor imaging outcomes in a large-scale population-based cohort. *Neuroimage*. 125:903–919.

Rosen AFG, Roalf DR, Ruparel K, Blake J, Seelaus K, Villa LP, Ciric R, Cook PA, Davatzikos C, Elliott MA *et al*. 2018. Quantitative assessment of structural image quality. *Neuroimage*. 169:407–418.

Satterthwaite TD, Ruparel K, Loughead J, Elliott MA, Gerraty RT, Calkins ME, Hakonarson H, Gur RC, Gur RE, Wolf DH. 2012. Being right is its own reward: load and performance related ventral striatum activation to correct responses during a working memory task in youth. *Neuroimage*. 61:723–729.

Satterthwaite TD, Wolf DH, Erus G, Ruparel K, Elliott MA, Gennatas ED, Hopson R, Jackson C, Prabhakaran K, Bilker WB *et al*. 2013. Functional maturation of the executive system during adolescence. *J Neurosci*. 33:16249–16261.

Satterthwaite TD, Elliott MA, Ruparel K, Loughead J, Prabhakaran K, Calkins ME, Hopson R, Jackson C, Keefe J, Riley M *et al*. 2014a. Neuroimaging of the Philadelphia neurodevelopmental cohort. *Neuroimage*. 86:544–553.

Satterthwaite TD, Shinohara RT, Wolf DH, Hopson RD, Elliott MA, Vandekar SN, Ruparel K, Calkins ME, Roalf DR, Gennatas ED *et al*. 2014b. Impact of puberty on the evolution of cerebral perfusion during adolescence. *Proc Natl Acad Sci USA*. 111:8643–8648.

Satterthwaite TD, Wolf DH, Roalf DR, Ruparel K, Erus G, Vandekar S, Gennatas ED, Elliott MA, Smith A, Hakonarson H *et al*. 2015. Linked sex differences in cognition and functional connectivity in youth. *Cereb Cortex*. 25:2383–2894.

Schmithorst VJ, Wilke M, Dardzinski BJ, Holland SK. 2005. Cognitive functions correlate with white matter architecture in a normal pediatric population: a diffusion tensor MR imaging study. *Hum Brain Mapp*. 26:139–147.

Smith SM. 2002. Fast robust automated brain extraction. *Hum Brain Mapp*. 17:143–155.

Smith SM, Brady JM. 1997. SUSAN—A new approach to low level image processing. *Int J Comput Vis*. 23:45–78.

Smith SM, Nichols TE, Vidaurre D, Winkler AM, Behrens TE, Glasser MF, Ugurbil K, Barch DM, Van Essen DC, Miller KL. 2015. A positive-negative mode of population covariation links brain connectivity, demographics and behavior. *Nat Neurosci*. 18:1565–1567.

Somandepalli K, Kelly C, Reiss PT, Zuo XN, Craddock RC, Yan CG, Petkova E, Castellanos FX, Milham MP, Di Martino A. 2015. Short-term test–retest reliability of resting state fMRI metrics in children with and without attention-deficit/hyperactivity disorder. *Dev Cogn Neurosci*. 15:83–93.

Swagerman SC, de Geus EJC, Kan KJ, van Bergen E, Nieuwboer HA, Koenis MMG, Pol HEH, Gur RE, Gur RC, Boomsma DI. 2016. The computerized neurocognitive battery: validation, aging effects, and heritability across cognitive domains. *Neuropsychology*. 30:53–64.

Swick D, Ashley V, Turken AU. 2008. Left inferior frontal gyrus is critical for response inhibition. *BMC Neurosci*. 9:102.

Tedesco AM, Chiricozzi FR, Clausi S, Lupo M, Molinari M, Leggio MG. 2011. The cerebellar cognitive profile. *Brain*. 134:3672–3686.

Tiedemann F. 1836. On the brain of the Negro, compared with that of the European and the Orang-Outang. Philosophical Transactions of the Royal Society of London. 126:497–527. (Stable URL: http://www.jstor.org/stable/108042 accessed: 11 October 2015 00:00 UTC).

Tremblay P, Dick AS. 2016. Broca and Wernicke are dead, or moving past the classic model of language neurobiology. *Brain Lang*. 162:60–71.

Tustison NJ, Avants BB, Cook PA, Zheng Y, Egan A, Yushkevich PA, Gee JC. 2010. N4ITK: improved N3 bias correction. *IEEE Trans Med Imaging*. 29:1310–1320.

Tustison NJ, Cook PA, Klein A, Song G, Das SR, Duda JT, Kandel BM, van Strien N, Stone JR, Gee JC *et al*. 2014. Large-scale evaluation of ANTs and FreeSurfer cortical thickness measurements. *Neuroimage*. 99:166–179.

Vandekar SN, Shinohara RT, Raznahan A, Roalf DR, Ross M, DeLeo N, Ruparel K, Verma R, Wolf DH, Gur RC *et al*. 2015. Topologically dissociable patterns of development of the human cerebral cortex. *J Neurosci*. 35:599–609.

Vakhtin AA, Ryman SG, Flores RA, Jung RE. 2014. Functional brain networks contributing to the Parieto-frontal integration theory of intelligence. *Neuroimage*. 103:349–354.

Wickham H. 2011. ggplot2. *Wiley Interdiscip Rev: Comput Stat*. 3(2):180–185.

Witelson SF, Beresh H, Kigar DL. 2006. Intelligence and brain size in 100 postmortem brains: sex, lateralization and age factors. *Brain*. 129:386–398.

Wang H, Suh JW, Das SR, Pluta JB, Craige C, Yushkevich PA. 2013. Multi-atlas segmentation with joint label fusion. *IEEE Trans Pattern Anal Mach Intell*. 35:611–623.

Wang JY, Abdi H, Bakhadirov K, Diaz-Arrastia R, Devous MD Sr. 2012. A comprehensive reliability assessment of quantitative diffusion tensor tractography. *Neuroimage*. 60(2):1127–1138.

Wang Z, Aguirre GK, Rao H, Wang J, Fernández-Seara MA, Childress AR, Detre JA. 2008. Empirical optimization of ASL data analysis using an ASL data processing toolbox: ASLtbx. *Magn Reson Imaging*. 26:261–269.

Wojtasik M, Bludau S, Eickhoff SB, Mohlberg H, Gerboga F, Caspers S, Amunts K. 2020. Cytoarchitectonic characterization and functional decoding of four new areas in the human lateral orbitofrontal cortex. *Front Neuroanat*. 14:2.

Wolff M, Vann SD. 2019. The cognitive thalamus as a gateway to mental representations. *J Neurosci*. 39:3–14.

Wu WC, Wong EC. 2007. Feasibility of velocity selective arterial spin labeling in functional MRI. *Journal of Cerebral Blood Flow and Metabolism*. 27:831–838.

Wu W, Jain V, Li C, Giannetta M, Hurt H, Wehrli FW, Wang DJJ. 2010. In vivo venous blood T1 measurement using inversion recovery true-FISP in children and adults. *Magn Reson Med*. 64:1140–1147.

Yan C, Gong G, Wang J, Wang D, Liu D, Zhu C, Chen ZJ, Evans A, Zang Y, He Y. 2011. Sex– and brain size-related small-world structural cortical networks in young adults: a DTI tractography study. *Cerebral Cortex*. 21:449–458.

Yoo K, Rosenberg MD, Hsu WT, Zhang S, Li CR, Scheinost D, Constable RT, Chun MM. 2018. Connectome-based predictive modeling of attention: comparing different functional connectivity features and prediction methods across datasets. *Neuroimage*. 167:11–22.

Yang H, Long XY, Yang Y, Yan H, Zhu CZ, Zhou XP, Zang YF, Gong QY. 2007. Amplitude of low frequency fluctuation within visual areas revealed by resting-state functional MRI. *NeuroImage*. 36:144–152.

Zang Y, Jiang T, Lu Y, He Y, Tian L. 2004. Regional homogeneity approach to fMRI data analysis. *Neuroimage*. 22: 394–400.

Zhang S, Laidlaw DH. 2006. Sampling DTI fibers in the human brain based on DWI forward modeling. IEEE Engineering in Medicine and Biology Society. *Annual Conference*. 4885–4888.

Zhang P, Niethammer M, Shen D, Yap PT. 2014. Large deformation diffeomorphic registration of diffusion-weighted imaging data. *Medical Image Analysis*. 18:1290–1298.